

RESEARCH ARTICLE

GMP-compliant manufacturing of biologically active cell-derived vesicles produced by extrusion technology

Hui-Chong Lau¹ | Dong Woo Han¹ | Jinhee Park¹ | Edwine Lehner² | Carina Kals² |
 Claudia Arzt³ | Elisabeth Bayer² | Daniela Auer² | Tanja Schally² | Eva Grasmann³ |
 Han Fang³ | Jae-Young Lee⁴ | Hyun Soo Lee⁴ | Jinah Han⁵ | Mario Gimona^{2,3,6} |
 Eva Rohde^{2,7} | Shingyu Bae¹ | Seung Wook Oh^{1,5} 

¹BioDrone Research Institute, MDimune Inc., Seoul, Korea

²GMP Unit, Spinal Cord Injury & Tissue Regeneration Centre Salzburg (SCI-TReCS), Paracelsus Medical University, Salzburg, Austria

³Transfer Centre for Extracellular Vesicle TheraLytic Technologies (EV-TT), Salzburg, Austria

⁴Department of Ophthalmology, Eunpyeong St. Mary's Hospital, College of Medicine, The Catholic University of Korea, Seoul, Korea

⁵BioDrone Therapeutics Inc., Seattle, USA

⁶Research Program "Nanovesicular Therapies", Paracelsus Medical University, Salzburg, Austria

⁷Department of Transfusion Medicine, University Hospital, Salzburger Landeskliniken GesmbH (SALK) and Paracelsus Medical University, Salzburg, Austria

Correspondence

Seung Wook Oh, BioDrone Research Institute, MDimune Inc., Seoul, Korea.
 Email: swoh@mdimune.com

Funding information

"EV-TT . Bpro" (Land Salzburg/WISS 2025), Grant/Award Number: 20102-F1900731-KZP; "EV-TT" (Land Salzburg/IWB/EFRE), Grant/Award Number: P1812596

Abstract

Extracellular vesicles (EVs) released by a variety of cell types have been shown to act as a natural delivery system for bioactive molecules such as RNAs and proteins. EV therapy holds great promise as a safe and cell-free therapy for many immunological and degenerative diseases. However, translation to clinical application is limited by several factors, including insufficient large-scale manufacturing technologies and low yield. We have developed a novel drug delivery platform technology, BioDrone™, based on cell-derived vesicles (CDVs) produced from diverse cell sources by using a proprietary extrusion process. This extrusion technology generates nanosized vesicles in far greater numbers than naturally obtained EVs. We demonstrate that the CDVs are surrounded by a lipid bilayer membrane with a correct membrane topology. Physical, biochemical and functional characterisation results demonstrate the potential of CDVs to act as effective therapeutics. Umbilical cord mesenchymal stem cell (UCMSC)-derived CDVs exhibit a biological activity that is similar to UCMSCs or UCMSC-derived EVs. Lastly, we present the establishment of a GMP-compliant process to allow the production of a large number of UCMSC-CDVs in a reproducible manner. GMP-compliant manufacturing of CDVs will facilitate the preclinical and clinical evaluation of these emerging therapeutics in anti-inflammatory or regenerative medicine. This study also represents a crucial step in the development of this novel drug delivery platform based on CDVs.

KEYWORDS

cell-derived vesicles, drug delivery platform, extrusion, GMP-compliant manufacturing, umbilical cord mesenchymal stem cell

1 | INTRODUCTION

Over the past decade significant progress has been made in the isolation of extracellular vesicles (EVs) for their therapeutic use (Cardoso et al., 2021; Nasiri Kenari et al., 2020; Wiklander et al., 2019). EV isolation can be achieved via several strategies utilising differential sedimentation (such as ultracentrifugation), filtration (ultrafiltration and size-exclusion chromatography) or affinity capture techniques. While all applied enrichment technologies suffer from certain shortcomings (labour intensive, not scalable, insufficient separation from co-purifying components, deformation of the final product), a major challenge that does not seem addressed easily by any of the enrichment technologies is that of yield (Li et al., 2021). EV-secreting cells release a limited number of EVs into the culture medium and the loss during the multistep purification process further diminishes the final yield.

This is an open access article under the terms of the [Creative Commons Attribution-NonCommercial License](https://creativecommons.org/licenses/by-nc/4.0/), which permits use, distribution and reproduction in any medium, provided the original work is properly cited and is not used for commercial purposes.

© 2022 The Authors. *Journal of Extracellular Biology* published by Wiley Periodicals, LLC on behalf of the International Society for Extracellular Vesicles.

An alternative method for generating EV-mimetics with higher yield and satisfactory reproducibility was developed using extrusion technology. Since its first description by Gho and his colleagues (Jang et al., 2013), many researchers have relied on the same method to generate and test these vesicles for their therapeutic potential. Such vesicles were named in a few different ways including exosome-mimetic nanovesicles (NVs), exosome mimetics (EMs), cell-derived nanovesicles (CDNs), cell-derived vesicles (CDVs), cell-engineered nanovesicles and cell-membrane vesicles (Choo et al., 2018; Goh, Zou, et al., 2017; Jang et al., 2013; Park et al., 2019; Zhang et al., 2021; Zhu et al., 2018), among which we propose 'cell-derived vesicles (CDVs)' to encompass all the vesicles produced based on the same extrusion process. CDVs can be prepared by extrusion of virtually any cells and display many similarities to EVs in terms of size and morphology as well as in the molecular composition of the surrounding membranes.

Diverse CDVs deliver cellular information to recipient cells and induce biological responses. Thus far, CDVs derived from immune cells, such as natural killer cells, T-cells and macrophages, showed promising therapeutic effects in cancer (Choo et al., 2018; Hong et al., 2021; Zhu et al., 2018). In addition, mesenchymal stem cell (MSC)-derived vesicles possess regenerative capacities in spinal cord injury, emphysema, vascular diseases, sepsis, inflammation, etc. (Kim et al., 2017, 2018; Ko et al., 2020; Kwon et al., 2019; Park et al., 2019). Furthermore, CDVs can be loaded with exogenous pharmaceutical molecules via electroporation or during the extrusion process (Goh, Lee, et al., 2017; Jang et al., 2013; Kalimuthu et al., 2018; Lunavat et al., 2016; Yang et al., 2016; Zhao et al., 2021). CDVs also exhibit natural targeting ability (Jang et al., 2013; Lee, Kyung, et al., 2020; Zhu et al., 2018), while maintaining the topology of plasma membrane proteins (Jang et al., 2013). Therefore, CDVs are not only regarded as an alternative to EVs with their high productivity that is more suitable for industrial scale but can also serve as an efficient drug delivery system for active pharmaceutical biomolecules in broad applications.

Here, we report that a large quantity of CDVs can be produced from umbilical cord MSCs (UCMSCs) through the manufacturing process established using the extrusion method and downstream purification processes. Comprehensive characterisation reveals that CDVs indeed display a high degree of similarity between EVs derived from the same cell source, including their therapeutic potentials as expected from UCMSCs or UCMSC-EVs. Finally, we describe the GMP-compliant manufacturing process to generate a CDV product that can be readily applied to multiple indications in regenerative or anti-inflammatory disease conditions.

2 | MATERIALS AND METHODS

2.1 | Primary isolation and expansion of human MSCs

UCMSCs were isolated as previously described (Pachler, Ketterl, et al., 2017). Briefly, whole cords were washed with PBS to remove contaminating blood cells before the cord stroma was cut into small pieces of 1–2 mm³. The tissues were transferred to a culture plate allowing them to dry-adhere to the plate surface before adding culture medium containing alpha-modified minimum essential medium (α -MEM; Sigma, #4526), 10% (v/v) pooled human platelet lysate (pHPL) and 5.5 mg/ml Dipeptiven (Fresenius-Kabi, #1330053). After 10–12 days, outgrowing UCMSC colonies became visible and cord tissues were removed. UCMSCs were detached enzymatically by the addition of TrypLE™ Select CTS™ (Thermo Fisher Scientific, #A12859-01), and further expanded in Nunc EasyFill™ Cell Factory™ systems (CF4, Thermo Fisher Scientific). Pooled HPL was prepared as previously described (Laner-Plamberger et al., 2015). In brief, expired platelet concentrates were lysed by several freeze/thaw cycles. Platelet fragments were pelleted by centrifugation (4000 × g, 15 min at room temperature) and aliquots of the supernatant were frozen at –30°C until use. For GMP-compliant manufacturing HPL was purchased from Aventacell (UltraGRO™-PURE GI GMP grade, #HPCHXCGLI50).

2.2 | Generation and purification of UCMSC-CDVs

CDVs were generated by using a custom-made extruder (ES50) and custom-made single-use extrusion cartridges. UCMSCs were expanded in 4-layer cell factories (CF4, Thermo Fisher Scientific) with a total growth surface of 2528 cm² in the media described above. The cell suspension was adjusted to 2.5 × 10⁵ cells/ml in PBS and was serially extruded through polycarbonate membrane filters with 10, 3 and 0.4 μm of pore sizes (Whatman) attached to ES50 extrusion devices. The cell suspension was filled into 50 ml sterile syringes mounted onto two inversely positioned and aligned Fusion 6000 high-pressure syringe pumps (Chemxy, USA). The volume was forced through each filter size three times. From the extruded crude CDV solution the total DNA content was determined, and DNA was digested by adding Benzonase endonuclease Safety Plus EMPROVE EXPERT (Sigma, #101697). The suspension was centrifuged for 10 min at 3000 × g at 18°C, and the supernatant was further processed by Tangential Flow Filtration (TFF) using D02-E750-05-S type TFF hollow fibre column filters (Repligen, USA). Diafiltration was used to achieve complete buffer exchange to PBS using a five-fold volume. After volume reduction and diafiltration, the remaining solution was centrifuged for 10 min at 3000 × g at 18°C. The cleared supernatant was filtered using a 0.22 μm for GMP-compliant

manufacturing, or a 0.45 μm syringe tip PES filter (Millipore, USA). The resulting suspension volume is between 250 μL and 1000 μL . Finally, CDVs were kept at -80°C until use.

2.3 | Manufacturing of UCMSC-EVs

Batches of EVs from UCMSCs were prepared according to Good Manufacturing Practice (GMP) as previously described (Desgeorges et al., 2020; Gimona et al., 2017; Pachler, Lener, et al., 2017; Warnecke et al., 2020). In brief, cells were cultured in fibrinogen-depleted culture medium at 5% CO_2 and 37°C . Upon reaching 60%–70% confluence, the growth medium was exchanged with the EV-depleted harvest medium containing 5% HPL. After 24 h, the conditioned medium was collected, centrifuged at $2500 \times g$ for 20 min at 18°C , and cleared via sterile filtration (0.22 μm). The resulting supernatant was concentrated and buffer-exchanged to PBS by TFF and diafiltration, respectively, using a 100 kDa hollow fibre column filter (Repligen, USA). Ultimately, EVs were enriched by ultracentrifugation at $120,000 \times g$ for 3 h at 18°C in a Sorvall model WX-80 using a fixed angle rotor model Fiberlite F37L-8 \times 100 (Angle = 25° , K Factor = 168). The resulting pellets were washed once with 10 ml PBS and subsequently resuspended in Ringer's Lactate. Resuspended EVs were subsequently centrifuged at $3000 \times g$ for 10 min at 4°C and the supernatant was sterile filtered (0.22 μm). EVs were tested for endotoxin levels, bacterial sterility and the presence of mycoplasma, and stored at -80°C until use. For characterisation work described in Figures 1–4, the same method was used as described above except that the harvested medium contained 4% of EV-depleted HPL and 1% of penicillin-streptomycin (Gibco, #15140122). Then, serial centrifugation was used to isolate EVs. First, cells and debris were removed at $300 \times g$ and $3000 \times g$ for 10 min at 4°C . Next, the conditioned medium was further centrifuged at $10,000 \times g$ for 30 min at 4°C to remove the apoptotic body. Finally, EVs were pelleted by ultracentrifugation at $120,000 \times g$ for 2 h at 4°C and resuspended in PBS.

2.4 | Nanoparticle tracking analysis (NTA), polydispersity index (PDI) and quantification for DNA, protein, and Benzonase

To determine the size and number of particles, samples were analysed using a Nanoparticle Tracking Device (ZetaView PMC 110 or PMX-220, Particle Metrix, Germany) in light scatter mode as previously described (Desgeorges et al., 2020). Prior to NTA analysis, the instrument was calibrated using Yellow/Green-labeled 100 nm polystyrene standard beads (1:1,000,000 dilution in ddH_2O). The minimum brightness was set to 20 arbitrary units (AU), temperature to 21.5°C , shutter to 70 AU, and sensitivity to 85 AU. CDVs or EVs were diluted in PBS to a concentration of $4\text{--}7 \times 10^7$ particles/ml. Data for two exposures at 11 measurement positions were acquired per sample. Polydispersity index (PDI) values were measured using a ZetaSizer NS (Malvern Instruments, UK). Samples were diluted in PBS to a total volume of 1 ml and measured in triplicate at 25°C with standard settings (Refractive Index: 1.331). The surface potential was measured using ZetaView. Zeta potential measurements were performed using samples diluted in DNase/RNase-free water. All the acquisition parameters were the same as above. Total protein and DNA amounts of CDVs and EVs were determined using a QuBit[®] 3.0 or 4.0 Fluorimeter instrument (Life Technologies, USA) according to the manufacturer's instructions. The residual Benzonase amount was detected using Benzonase ELISA kit II Millipore, USA, #101681) according to the manufacturer's instructions.

2.5 | Western blotting

CDVs or EVs were incubated with an equal volume of Laemmli sample buffer (Bio-Rad Laboratories, #161-0737) supplemented with 2-Mercaptoethanol (Bio-Rad Laboratories, #161-0710) at 95°C for 5 min. An equal amount of total proteins (1 μg for all except CD81 and CD9, in which 8 μg was used) from UCMSCs, UCMSC-CDVs and UCMSC-EVs were then separated on 4%–15% gradient polyacrylamide gels (Bio-Rad Laboratories, #456-1084) and transferred onto nitrocellulose membranes (Bio-Rad Laboratories, #170-4158). Precision Plus Protein[™] Dual Color Standards (Bio-Rad Laboratories, #1610374) served as the protein size marker. Then, the nitrocellulose membranes were incubated in Ponceau-S solution (0.1% in 5% acetic acid; Sigma, #P7170) for 5 min and rinsed in distilled H_2O for 5 min. Next, membranes were blocked with 5% non-fat dry milk in Tris-buffered saline containing 0.1% Tween-20 (TBS-T) for 1 h at room temperature and probed with primary antibodies: anti-CD63 (Life Technologies, #10628D), anti-CD9 (Life Technologies, #10626D), anti-LAMP1 (Sino Biological, #11215-R107), anti-CD81 (Abcam, #ab79559), anti-calnexin (Abcam, #ab92573), anti-CD29 (Abcam, #ab134179), anti-GM130 (Abcam, #ab52649), anti-citrate synthase (Abcam, #ab233838), anti-lamin B1 (Abcam, #ab220797), anti-flotillin-1 (Cell Signaling, #18634S) at 1:2500 and CD73 (Cell Signaling, #13160S) at 1:1000. The membranes were then washed three times with TBS-T and incubated with secondary antibodies, goat anti-mouse (Novus Biological, #NB7539) for CD63, CD81 and CD9; goat anti-rabbit (Novus Biological, #NB7160) for CD29, LAMP1, flotillin-1, lamin B1, calnexin, citrate synthase and GM130; or anti-rabbit IgGs, HRP linked

(Cell Signaling, #7074S) for CD73 at 1:1000 to 1:5000 ratio. Documentation was performed using ChemiDoc with ECL Prime (Bio-Rad Laboratories, USA).

2.6 | MACSPlex surface protein profiling

The bead-based multiplexed flow cytometry-based MACSPlex Exosome Kit (Miltenyi Biotec, Germany) is an assay for the analysis of surface markers present on EVs. To characterise CDVs or EVs, we used the MACSPlex kit according to the manufacturer's instructions and following a validated standard operating procedure (SOP) with 5×10^7 to 5×10^8 total particles as input (Warnecke et al., 2020). Briefly, CDVs were incubated with 37 capture bead populations coated with different antibodies against potential EV surface antigens. Then, the beads were counterstained with an APC-conjugated tetraspanin mix (anti-CD9, anti-CD63 and anti-CD81). After data acquisition using a FACSCanto II instrument (BD Biosciences, USA), each bead intensity was normalised against the mean value of median fluorescence intensity (MFI) of three tetraspanin markers (CD9, CD63 and CD81) and named arbitrary unit (AU). Isotype control normalisation was performed as described (Wiklander et al., 2018). To estimate the expression level of CD73 and CD90, BV421-conjugated anti-CD73 or anti-CD90 antibodies were used (BD Biosciences, #562431 and #562556, respectively) instead of APC-conjugated tetraspanin mix.

2.7 | Cryo-TEM and SEM analysis

Briefly, CDVs and EVs were first transferred onto a 20 nm-mesh grid. The grids were incubated at -196°C for 2 h using Vitrobot (FEI, USA) prior to imaging with cryogenic transmission electron microscopy (Cryo-TEM; Tecnai, F20 G2, FEI, USA). Five different batches of CDVs and two batches of EVs were used to collect TEM images. At least three TEM images (approximate dimension of $1.9 \mu\text{m} \times 1.9 \mu\text{m}$) that contained the minimum eight vesicles (up to 51 vesicles) with a clear morphology and lipid bilayer structure per image were selected from each batch of samples and used to classify vesicles. Finally, a total of 645 CDVs and 165 EVs were classified into single- or multi-layered membrane vesicles. For scanning electron microscopy (SEM), CDVs and EVs were fixed with 2.5% of glutaraldehyde overnight, and images were taken by using FE-SEM Merlin, (Carl Zeiss, Germany).

2.8 | Membrane topology

CDVs were treated with proteinase K (Sigma, #P6556) at 0.05 or 0.2 μg of proteinase K per microgram of protein. The mixture was incubated for 1 h at 37°C with gentle vortexing every 15 min. The proteinase K activity was then quenched by heating the mixture at 90°C for 5 min. The membrane topology was confirmed by Western blotting using anti-CD29 antibodies with epitope at N- (Abcam, #ab134179) and C-terminal (Abcam, #ab183666).

2.9 | Cellular uptake assays

1×10^{11} particles of UCMSC-CDVs or -EVs were labelled with 5 μM DiR (Invitrogen, #D12713) by incubating at 37°C for 30 min in 1 ml reaction volume. Excessive DiR was removed by the PD-10 desalting column packed with Sephadex G-25 resins (GE Healthcare, USA) following the manufacturer's instructions. Control groups for CDVs and EVs were prepared in the same manner with PBS in the absence of DiR. BT549 cells (triple-negative breast cancer cell line) were seeded on a 24-well plate at 4×10^4 cells/well the day before use. The next day, DiR-labelled CDVs (DiR-CDVs), EVs (DiR-EVs), and the control groups were added to the cells at 1×10^5 particles per cell concentration and incubated at 37°C for 1, 3, 6, 18, 24 and 48 h. To test additional cell lines, HUVEC, NHDF and HEK293 were used and analysed after incubating for 24 h. Cells were labelled with 5(6)-carboxyfluorescein diacetate N-succinimidyl ester (CFSE; Abcam, #ab113853) at a final concentration of 5 μM for 30 min in serum-free media to normalise the respective cell mass. To digest surface proteins, CDVs and EVs were treated with proteinase K at 0.2 μg proteinase K/ μg protein before labelling with DiR. DiR-CDVs and DiR-EVs were added to BT549 cells at 1×10^5 particles per cell concentration and incubated at 37°C for 24 h. For the surface protein blocking, 2×10^9 particles of DiR-CDVs and DiR-EVs were treated with different antibodies against CD63, CD81, CD9, CD29 and LAMP-1 (see above in surface marker analysis) at 1:100 (high); 1:1000 (medium) and 1:10,000 (low) for 30 min at 4°C in the dark. The fluorescence intensity was measured using a flow cytometer (Sony, Japan) to determine the uptake efficiency. The fluorescence intensity of either proteinase K-untreated or antibody-untreated DiR-UCMSC-CDVs was used to normalise each data for comparative analysis. For confocal microscopy, BT549 cells treated with DiR-CDVs or DiR-EVs were collected at 3, 6 and 24 h after incubation and fixed with paraformaldehyde. Then, cells were incubated with anti- β -tubulin antibody (Abcam, #ab108342) overnight at 4°C , followed by incubation with secondary antibody (Alexa Fluor 488-conjugated anti-rabbit IgG; Abcam, #ab150077) in room temperature for 1 h and

counterstaining with Hoechst (Vector Laboratories, #H-1800). Fluorescence images were obtained using a confocal microscope (Leica, Germany).

2.10 | Retinal penetration assay

CDVs and EVs were incubated at 2×10^{11} particles/ml with $5 \mu\text{M}$ of Vybrant DiD Cell-Labeling Solution, (Invitrogen, #22887) in 2% ethanol for 60 min at 37°C . After incubation, the excess dye was removed using Zeba Spin™ desalting column, 40K MWCO (Thermo Fisher Scientific, USA), following the manufacturer's instructions. The total fluorescence of DiD-labelled CDVs and EVs was measured using a microplate reader (SpectraMax M2, Molecular Devices, USA). C57BL/6 mice (8–9 weeks old; five animals in each group) were anaesthetised, and $1.5 \mu\text{l}$ of DiD-labelled CDVs or EVs were injected into the right eye (intravitreal injection) using the Hamilton microinjector needle (Hamilton, USA). PBS was injected as the control group. The mice were sacrificed at 6 and 24 h post-injection. The eyeball was removed and fixed in 4% paraformaldehyde with 30% sucrose for cryosection. The tissue sections were obtained at $7 \mu\text{m}$ thick and stained with anti-RPE65-Alexa Fluor 488 (Santa Cruz, USA, #sc-390787) to label retinal pigment epithelium (RPE) at 4°C overnight. The next day the sections were washed three times with 0.025% Triton-X in PBS. Finally, the tissue sections were mounted with VECTASHIELD mounting solution containing DAPI (Vector Labs, UK, #H-1200-10) and visualised under the epifluorescence microscope (Zeiss, Germany). The fluorescence intensity of DiD-labelled vesicles in the retina was measured at two different time points and normalised against the total fluorescence of injected materials as described above. All animal studies were approved by the Animal Research Ethics Committee of the Catholic University of Korea (IACUC approval #EPSMH20201704FA).

2.11 | CD73 activity assay

The enzymatic activity of CD73 was determined by incubating $10 \mu\text{l}$ of CDVs (approximately 3×10^8 – 3×10^9 particles) in 10 mM HEPES buffer containing 2 mM MgCl_2 with $10 \mu\text{M}$ AMP (Sigma, #01930) for 20 min at 37°C . The amount of AMP consumption was detected with the AMP-Glo™ Assay Kit (Promega, USA) according to the manufacturer's protocol and measured with a Spark® multimode microplate reader (Tecan, Austria). Two nanograms rhCD73 (Sigma, #N1665) were used as positive control and AMP-CP (Sigma, #M8386) as CD73 inhibitor.

2.12 | Immunomodulation assay

To investigate the immunomodulatory activity, the capacity to inhibit T-cell proliferation *in vitro* was studied as described previously (Pachler, Ketterl, et al., 2017). Stimulation of T-cell proliferation was achieved by incubation with CD3/CD28 antibody beads (Dynabeads™ Human T-Activator CD3/CD28 for T-Cell Expansion and Activation, Thermo Fisher Scientific, #11131D). CFSE-pre-labelled human peripheral blood mononuclear cells (PBMC) were stimulated with CD3/CD28 and co-cultured with UCMSC-CDVs or UCMSC-EVs for 72 h at a ratio of 0.5 – 1×10^4 particles per cell (3×10^5 cells per assay) as previously described (Trickett & Kwan, 2003). Six different batches of CDVs produced in independent production runs were used in comparison with a single batch of EVs. The percentage of inhibition of fluorescently labelled CD3 T-cell proliferation was analysed by flow cytometry in triplicates.

2.13 | Pro-inflammatory cytokines

The level of pro-inflammatory cytokines, such as IFN- γ , IL-1 β , IL2, IL4, IL-6, L-8, IL-10, IL-12p70, IL13 and TNF- α , from various preparations was analysed using V-Plex and U-Plex human multiplex immunoassay kits on the MSD platform (Meso Scale Diagnostics, USA) according to the manufacturer's instructions.

2.14 | Flow cytometric analysis of UCMSCs

To demonstrate the MSC identity of the parental cells at the time of collection, immuno-phenotyping and viability analysis of MSC was carried out according to the proposed surface marker profile for defining MSC identity as published by the International Society of Cell Therapy (ISCT) in 2006 (Dominici et al., 2006). Collected cells were centrifuged ($300 \times g$ for 7 min), resuspended in 5% v/v sheep serum-containing blocking buffer to reach a concentration of 1.5×10^7 cells/ml, and incubated for 20 min at 4°C in the dark. 3×10^5 cells were stained with mouse anti-human monoclonal antibodies against CD90 (Beckman Coulter,

#IM1839U), CD105 (Life Technologies, #MCHD10505), CD14, CD34, CD45, CD73, HLA-II (DR) (BD Biosciences; #345785, #345802, #345808, #550257, #347400, respectively), or corresponding isotype controls for 25 min at 4°C in the dark. Samples were washed in PBS, resuspended in 100 µl 7AAD-containing PBS (1:10 dilution, 0.0005 w/v % final concentration), and stained for 10 min at room temperature. Finally, 400 µl cold PBS was added and the samples were measured immediately using a FACSCanto II flow cytometer (BD Biosciences, USA) until 10,000 live cell events were recorded per staining. Blue (488 nm) and red (633 nm) laser-excited fluorescence signals were detected with the following standard light filters: FITC: 530/30 nm; PE: 585/42 nm; APC: 660/20 nm; 7AAD: 670LP. Results were analyzed with WinList software 8.0 (Verity Software House, USA). FSCA -SSCA dot plot analyses were applied for debris exclusion, and a doublet discrimination panel was set on the FSC channel for the detection of the height and width of the fluorescence signals. The ratio of the viable cells was determined on the SSC-7AAD dot plot.

2.15 | Safety tests of CDVs

The bacterial endotoxins were tested in the CDVs according to Eu. Ph. 2.6.14, using the endosafe[®]-PTS[™] system (Charles River, USA), and the mycoplasma test for CDVs was assessed according to the Eu. Ph. 2.6.7 using the e-Myco[™] VALiD² Mycoplasma PCR Detection Kit (iNtRON Biotechnology, Republic of Korea). All GMP-compliant CDV batches were tested for endotoxin levels and sterility, according to Eu. Ph. 2.6.1 (AGES Graz, Austria), and mycoplasma levels (EUROFINS, Italy) according to Pharm Eur. The presence of human pathogenic virus and mycoplasma as well as sterility from the established Master and Working Cell banks were tested according to Pharm Eur (Virusure, Austria).

3 | RESULTS

3.1 | Manufacturing of CDVs by extrusion

Although many researchers have shown the therapeutic value of CDVs, the scale of extrusion has been limited due to the extruder volume, typically relying on 1 ml-syringe extruders (Avanti Polar Lipids, USA; NanoSizer[™] Mini[®], T&T Scientific Corporations, USA). Therefore, we first invented an extruder that can process a substantially large volume of cell culture at once by adopting a similar syringe-plunger concept. The new extruder consists of four pairs of 50 ml disposable syringes connected in parallel, centre units containing membrane filters housed in a metal case along with supporters, multi-hole discs, and O-rings, a syringe mount that holds all four sets of centre units and syringes connected to them, and two syringe pumps (Figure 1a). By the action of two pumps, cell suspensions in each syringe get passed through membrane filters bidirectionally. Therefore, the new extruder was named ES50 (Extruder, Syringe type, 50 ml/syringe). Finally, software was developed to assist in the control of the flow rate and the number of extrusions in a more automated fashion. An assembled ES50 is shown in Figure 1a.

The manufacturing process was developed using an ES50 extruder (Figure 1b). The upstream process consists of the UCMSC expansion and cell extrusion. UCMSCs were grown and harvested as previously described (Rohde et al., 2019) and resuspended in the desired buffer at the pre-determined density. Key extrusion parameters, such as cell density, flow rate, trans-membrane pressure difference, choice of pore sizes for membrane filters, the number of extrusions per each pore size, etc., were empirically determined to give the best extrusion outcome through rigorous optimisation. For UCMSCs, serial extrusions are carried out typically by passing cells through three different membrane filters, with pore sizes of 10 µm, 3 µm and 0.4 µm, three times each (total 3 × 3 = 9 extrusions). In the downstream process, the post-extrusion mixture ('crude CDVs') is first treated with Benzonase[®] endonuclease to eliminate DNAs or other nucleic acids exposed to the mixture by disrupting cell membranes. The mixture is then concentrated, and the extra proteins, nucleic acids and other cellular debris remaining outside CDVs are purified using the TFF method, followed by the final filtration using 0.22 or 0.45 µm filters.

The resulting products ('purified CDVs') are monitored using a series of analytical methods to assess the quality and consistency of the product. The common quality attributes are described in Figure 2 and Table 1. The parental cells for extrusion, UCMSCs, are characterised for the expression of surface markers for quality assurance prior to extrusion as well. Most importantly, the vesicle yield obtained from extrusion was calculated by measuring particle numbers using a nanoparticle tracking analysis device (ZetaView) and compared to that of EVs purified from conditioned media by the serial ultracentrifugation method. As shown in Figure 1c, the productivity of extrusion (5.1×10^4 – 1.2×10^5 particles/cell) was 18.2 times higher on average compared to EVs (2.5×10^3 – 5.5×10^3 particles/cell), even though we used far more stringent purification method for CDVs.

3.2 | Physicochemical characterisation of CDVs

To understand the characteristics of CDVs produced from ES50 extruders, we compared the physical properties of CDVs with those of EVs secreted naturally from the cells. As reported elsewhere, most particles of both CDVs and EVs were measured

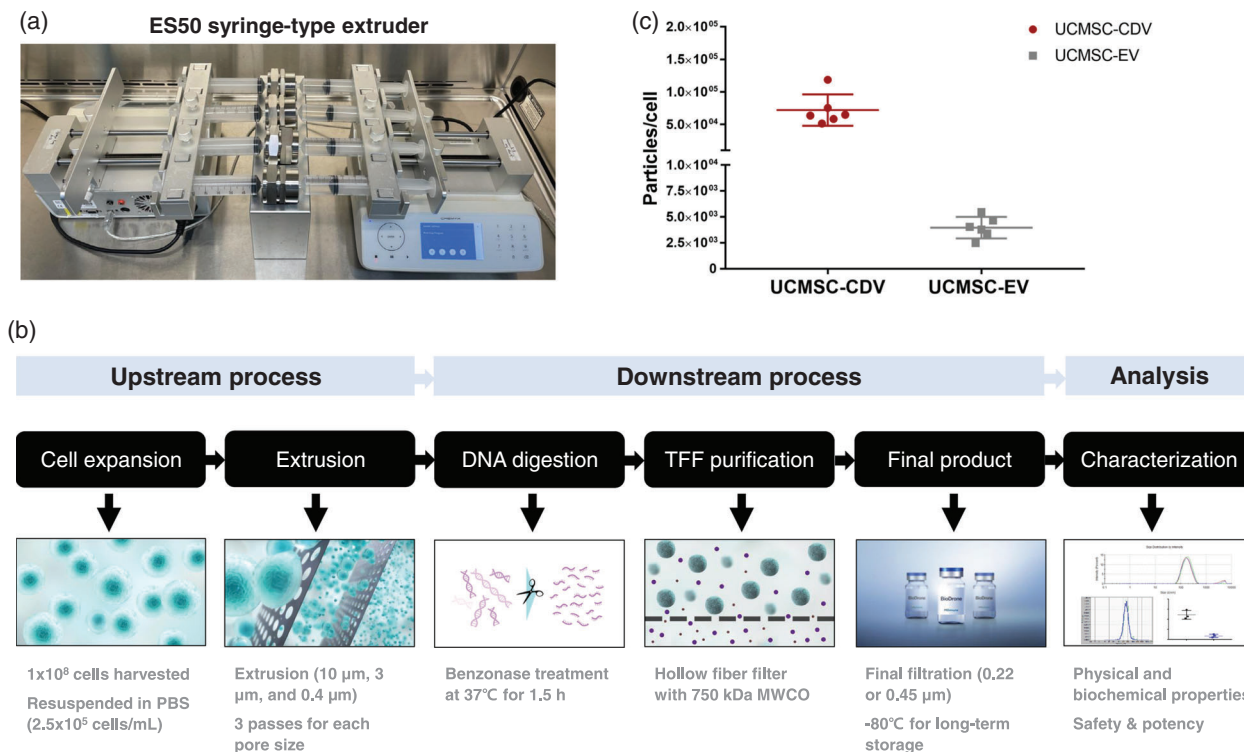


FIGURE 1 Manufacturing workflow of cell-derived vesicles (CDVs). (a) ES50 system developed at MDimmune. The new extruder consists of four pairs of 50 ml disposable syringes, centre units containing membrane filters and two syringe pumps. (b) Manufacturing workflow for UCMSC-CDVs. UCMSCs are harvested and resuspended in PBS at 2.5×10^5 cells/ml. Serial extrusions are carried out to convert cells into CDVs, followed by DNA digestion and separation of residual impurities. The final CDV products are stored at -80°C until further use. (c) The productivity comparison between CDVs and EVs from UCMSCs. The particle yield was measured by NTA using the ZetaView technology and the particle/cell was plotted from six different batches of CDVs or EVs derived from UCMSCs. Data represent the mean \pm SD

in the range of 50–200 nm in diameter, with the mean size of 142.8 ± 3.5 and 153.5 ± 8.8 , respectively (Figure 2a). CDVs also showed a similar but slightly lower polydispersity index (PDI) of 0.28 ± 0.02 when compared to EVs, 0.39 ± 0.05 as measured by the Dynamic Light Scattering technique (Figure 2b). We also compared the particle size distribution between CDVs and EVs (Figure 2c). Both vesicles showed a highly overlapping size distribution profile, with approximately 95% of vesicles ranging from 50 to 250 nm (Figure S1), suggesting that the serial extrusion process produces nanovesicles highly similar in physical properties to EVs.

Next, we examined the expression pattern of key surface markers of CDVs and EVs. To gain a better understanding of how CDVs are generated, apparently, via different mechanisms from EVs (Lee, Kang, et al., 2020), we selected representative membrane protein markers for the plasma membrane and each sub-cellular organelles as well as well-established EV markers: integrin beta-1 (CD29) and flotillin-1 for the plasma membrane, calnexin for endoplasmic reticulum (ER), GM130 for Golgi apparatus, citrate synthase for mitochondria, lysosomal-associated membrane protein 1 (LAMP1) for lysosome, lamin B1 for nucleus and three tetraspanin proteins (CD63, CD81, CD9) for EV markers. Overall, CD63, flotillin-1 and subcellular organelle markers such as LAMP1, calnexin and GM130 were highly enriched in CDVs compared to EVs or source cells (Figure 2d). EVs contain more CD9 and CD81 than CDVs, and some subcellular organelle markers such as lamin B1 and citrate synthase were scarce in both CDVs and EVs (Figure 2d). These results are consistent with the previous findings in CDVs and EVs (Lee, Kang, et al., 2020). Calnexin is often used as a negative marker to determine the purity of EVs (Dooley et al., 2021), whereas it was reported to be contained in CDVs (Lee, Kang, et al., 2020). Proteomics analysis also revealed the innate difference between CDVs and EVs (Nasiri Kenari et al., 2019).

Furthermore, the key findings were verified using flow cytometry. A comparison of UCMSC-EVs with UCMSC-CDVs, using a bead-based multiplex analysis (MACSplex Exosome Kit, human, from Miltenyi Biotec), reveals a highly similar yet distinctive profile for each vesicle entity (Figure 2e). While common EV traits such as CD9, CD29, CD63 and CD81 are abundantly detected on both EVs and CDVs, the level of CD44 (the receptor for hyaluronic acid) is much higher on CDVs. By contrast, the chondroitin sulphate proteoglycan MCSP (also known as NG2 or CSPG4) is exclusively detected on the surface of UCMSC-EVs. Notably, MCSP has been suggested as an identity and quality marker for MSC-derived EVs (Barilani et al., 2019). Overall, the MACSplex analyses recapitulated the expression pattern in CDVs and EVs with reproducible differences for the canonical EV surface markers CD63, CD81 and CD9, as observed by Western blotting (Figure 2d,e). The low levels of HLA-ABC (but not

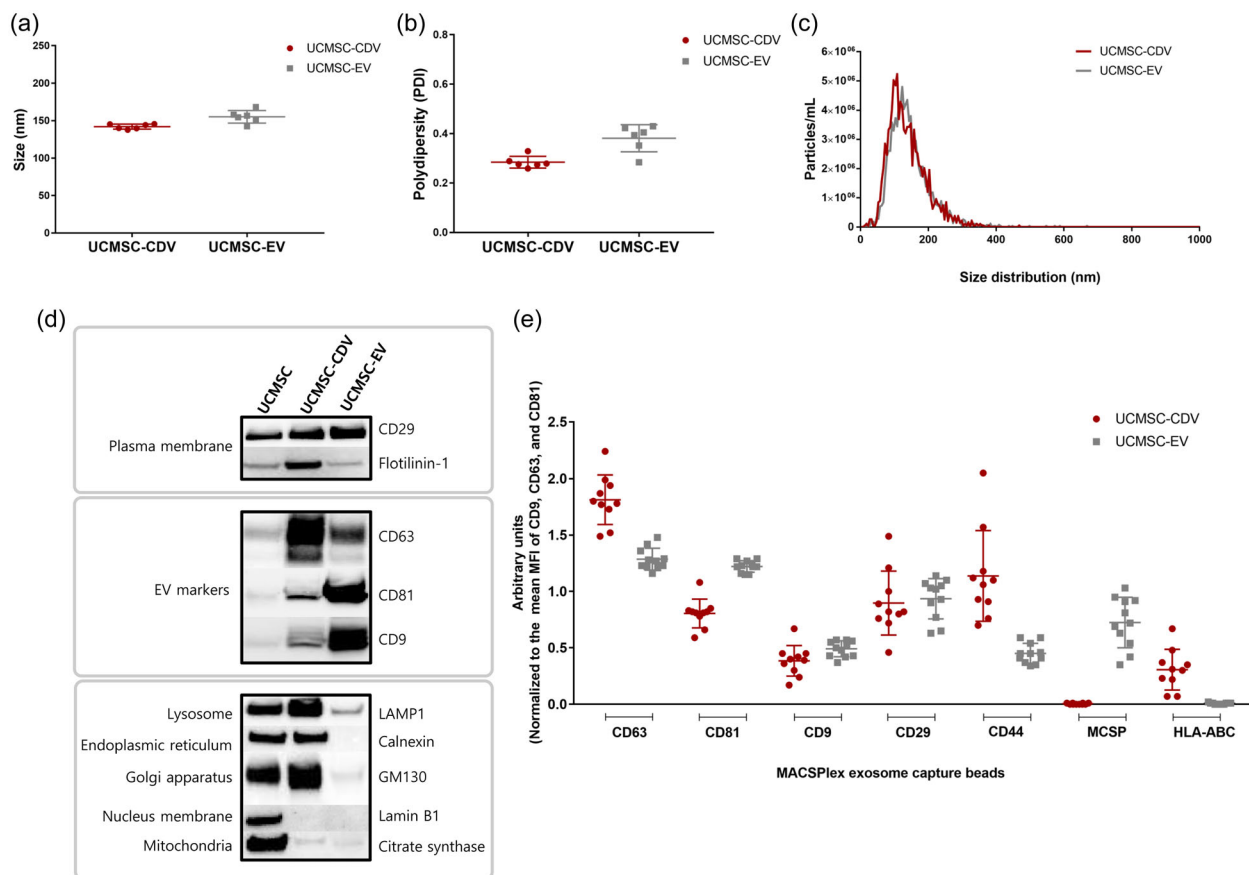


FIGURE 2 Physicochemical characterisation of CDVs. (a–c) Particle size and size distribution. CDVs produced by cell extrusion exhibit similar size and size distribution as secreted EVs. The size (a) and PDI (b) were measured from six different batches of CDVs or EVs derived from UCMSCs. Data represent the mean \pm SD. A representative distribution pattern is shown to compare the size distribution of CDVs and EVs (c). (d) Expression of EV-specific and subcellular organelle markers. The expression level of various marker proteins representing plasma membrane (CD29, Flotillin-1), EV membrane (CD63, CD81, CD9), and subcellular organelle membranes (LAMP1, Calnexin, GM130, Lamin B1, Citrate synthase) were determined by Western blotting analyses using the equal amount of total proteins from UCMSCs, UCMSC-CDVs and UCMSC-EVs ($N = 3$ or more). Representative images are shown for each marker. (e) Analysis of surface marker expression using MACSPlex Exosome kit. CDVs and EVs were bound to beads against representative surface markers including CD63, CD81, CD9, CD29, CD44, MSCP and HLA-ABC, and counterstained with a mixture of APC-labelled antibodies (CD63, CD81, CD9). The signal intensity for each marker was normalised to the mean of MFI of each tetraspanin marker (CD63, CD81, CD9). Data represent the mean \pm SD

TABLE 1 Key manufacturing and critical processing parameters

Parameter	Category	Technology	Acceptance criteria
Identity	MSC profile for producer cells at the time of harvest	Flow cytometry	>90% for positive markers (CD73, CD90, CD105) <2% for negative markers (CD14, CD19, CD45, HLA-DR)
	Particle Size	NTA	110–180 nm
	Particles/cell	NTA	$>1 \times 10^4$ particles/cell
	Protein amount	Fluorometry	<500 $\mu\text{g}/\text{ml}$
	Residual DNA	Fluorometry	>99% removal
	Surface marker profile	Flow cytometry (MACSPlex)	Positive (>0.2 AU) for CD9, CD29, CD63, CD73, CD81 and CD90
	Residual benzonase	ELISA	>99.9% removal
Safety	Endotoxins	LAL Test (Chromogen Kinetic Method)	<5 EU/ml
	Mycoplasma	Indicator Cell Culture Method	Negative
	Sterility	Membrane Filter Method	Negative
	Proinflammatory Cytokines	Commercial Kit	No acceptance criterion – for informative purposes only
Potency	CD73 enzymatic activity	Custom Modified Commercial Kit	$> 2 \times 10^{-8}$ μM AMP consumption/particle

HLA-DR) that are detected only on the surface of CDVs are in agreement with the findings that undifferentiated MSCs are moderately positive for HLA-ABC (but almost completely negative for HLA-DR) and that expression of HLA-ABC is observed on the plasma membrane in more than 90% of MSCs, independently of the tissue of origin (Petrenko et al., 2020). The rest of the marker proteins included in the MACSPlex kit are not discussed here as they did not show a consistent level of expression above the threshold we set (>0.2 AU, see Section 2.6).

Also, the flow cytometry analysis using aldehyde sulphate beads, commonly used to analyse the surface marker expression on nanovesicles, reports similarly high levels of key markers that were substantially different in expression level between UCMSC-CDVs and UCMSC-EVs by Western blotting, indicating that the conventional flow cytometry analysis may be a handy tool for determining major markers, but not a quantitative way to reveal subtle differences in surface protein expression of nanovesicles (Figure S2).

3.3 | A possible mechanism underlying extrusion and morphology of CDVs

We further examined the morphological structure of CDVs in comparison with EVs. CDVs and EVs shared a similar morphology with characteristic lipid bilayer structure surrounding the vesicles as revealed under the high-resolution Cryo-TEM (Figure 3a,b), consistent with previous reports (Goh, Zou, et al., 2017; Jang et al., 2013; Li et al., 2021; Nasiri Kenari et al., 2019). Round-shaped vesicles were the major form of CDVs as well as EVs. Further image analysis showed that more than 85% of vesicles were single-layered vesicles while the rest 15% were double- or multi-layered vesicles (Figure 3e). A similar phenomenon of the coexistence of single- and multi-layered vesicles was previously reported in EV research (Cvjetkovic et al., 2016; Emelyanov et al., 2020). The SEM imaging technique also revealed that most particles have similar sizes and shapes (Figure 3c,d), which is consistent with the size distribution results shown above (Figure 2c). This indicates that the CDVs and EVs have highly similar morphological characteristics.

We then investigated the membrane topology of CDVs produced by extrusion. The CD29 is a transmembrane protein with N- and C-terminal domains projecting toward extracellular and intracellular surfaces, respectively. We hypothesised that the CDVs with the original ('correct') membrane topology, after digestion of extracellular (thus extravesicular) surface with proteinase K, would not be detected by an anti-CD29 antibody with the N-terminal epitope ('extra' epitope), whereas partially digested bands including a 12 kDa band (fully digested) would show up by incubation with an antibody with the C-terminal epitope ('intra' epitope; Figure S3). As predicted, the original 130 kDa band of CD29 proteins largely disappear with proteinase K treatment as shown using antibodies against both extra and intra epitopes, while a ladder of partially digested proteins, including the 12 kDa band, show up when incubated with antibody against the intra epitope (Figure 3f). If CDVs remain mostly in the inversed topology, the incubation with extra epitope would have resulted in a high level of the high-molecular-weight band (~ 120 kDa) while leaving almost no detectable bands with antibody against intra epitope. The relatively low level of undigested CD29 (130 kDa in the L or H column) is probably due to the multi-layered vesicles (up to 15% of total vesicles) that may prevent the digestion of CD29 residing on the inner membrane of CDVs. When flotillin-1, with no extravesicular domains, was subjected to the same assay, flotillin-1 remained unaffected by proteinase K treatment (Figure 3f). Taken together, these results strongly suggest that CDVs produced from the intermediate-scale extruder (ES50) also maintain the original topology as donor cells after the extrusion process as previously shown using a small-scale extruder (Jang et al., 2013).

As illustrated in Figure 3g, the extrusion process is a highly productive way of generating EV-like nanovesicles with the original topology by utilising multiple sources of lipid membranes including those contributed by the subcellular organelles (Figure 2d). We believe that this largely accounts for the higher productivity of CDVs compared to natural EVs (Figure 3g).

3.4 | Cellular uptake and tissue penetration

To further demonstrate the therapeutic potential of CDVs in regulating cellular activities or serving as drug carriers, we explored the cellular uptake properties of CDVs. We used a breast cancer cell line, BT549, as the recipient cell and evaluated the degree of cellular uptake of CDVs from as early as 15 min to 48 h. The uptake efficiency of fluorescently labelled CDVs was determined by flow cytometry and compared to the same number of EVs prepared in the same way. At each time point, CDVs showed increased cellular uptake compared to EVs (Figure 4a). A similar increase was observed in other recipient cells tested, such as human umbilical vein endothelial cells (HUVEC) and normal human dermal fibroblasts (NHDF) (Figure 4b). Interestingly, the difference between CDVs and EVs remained approximately two-fold across different cell types. In contrast, HEK293 showed a low level of cellular uptake for both CDVs and EVs (Figure 4b). Results from confocal microscopy analysis also verified these findings by showing a substantially increased cellular uptake of CDVs (red) compared to EVs (Figure 4c). No apparent cytotoxicity was noticed upon treatment of CDVs or EVs (Figure S4C).

Next, we investigated the possible mechanism underlying the enhanced cellular uptake by CDVs. We first performed the cellular uptake assay after digesting surface proteins by proteinase K treatment. Our results showed that the cellular uptake

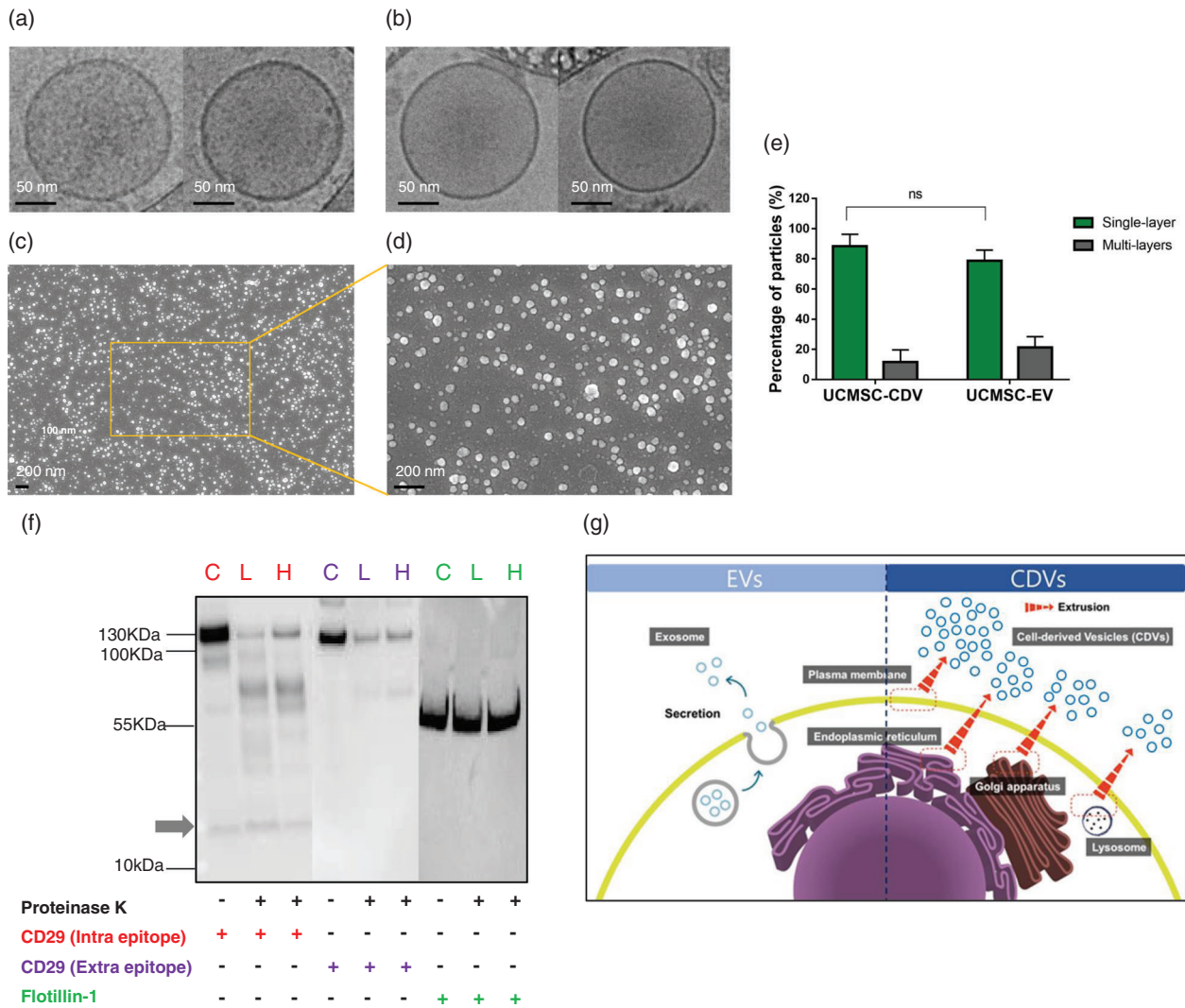


FIGURE 3 Morphology, membrane topology, and production mechanism of CDVs. (a and b) Representative Cryo-TEM images of CDVs and EVs derived from UCMSCs. Scale bar: 50 nm. (c and d) Representative SEM images of UCMSC-CDVs. Scale bar: 200 nm. (e) Quantitation of single- vs. multi-layered CDVs from selected Cryo-TEM images. Five different batches of CDVs and two batches of EVs were used to collect TEM images. At least three TEM images (approximate dimension of $1.9 \mu\text{m} \times 1.9 \mu\text{m}$) that contained the minimum eight vesicles (up to 51 vesicles) with a clear morphology and lipid bilayer structure per image were selected for each batch of samples. All the vesicles from the selected TEM images were then examined individually to classify them into single- or multi-layered structures (the total number of vesicles analysed: CDV, $n = 645$; EV, $n = 165$). Data represent the mean \pm SD. ns. Not significant from unpaired *t*-test. (f) Analysis of the membrane topology of CDVs using membrane proteins (CD29, large extravesicular domain; Flotillin-1, no extravesicular domain). UCMSC-CDVs were digested with proteinase K at two different concentrations (C: no treatment; L and H: 0.05 (low) and 0.2 (high) μg of proteinase K per μg of protein, respectively) and subjected to Western blotting with anti-CD29 antibodies with two different epitopes, denoted as 'intra' for C-terminal epitope (facing intracellular space) or 'extra' for N-terminal epitope (facing extracellular space), as well as anti-Flotillin-1 antibody as a control. The intact CD29 band (130 kDa) largely disappeared with proteinase K treatment as shown by both anti-CD29 antibodies, while partially digested proteins, including 12 kDa (fully digested) showed up with anti-CD29 ('intra'). Flotillin-1, without extravesicular domains, was unaffected by proteinase K treatment. (g) The current hypothesis of CDV production. A schematic diagram shows the possible mechanism of the high productivity of CDVs compared to EVs, attributed to the utilisation of multiple sources of lipid membranes including those of subcellular organelles

of CDVs was reduced to nearly half of the untreated control, while a relatively smaller reduction was observed in EVs upon digestion of surface proteins (Figure 4d), indicating that surface proteins play a critical role in the improved uptake of CDVs. We subsequently inhibited membrane proteins enriched in CDVs or EVs by using specific antibodies against those proteins at different concentrations. Remarkably, the cellular uptake of CDVs was reduced to approximately 50% of the untreated control by using a high concentration of anti-CD63 antibody, similar to that with proteinase K treatment (Figure 4d, e). The blockade of LAMP1 resulted in a similar decrease in cellular uptake in a dose-dependent manner but was slightly less prominent than CD63 (Figure 4e). The results show that CD63 and LAMP-1 are associated with the cellular entry of CDVs more strongly than other tetraspanin proteins (CD81, CD9 or CD29). Considering that CD63 and LAMP1 are among the most abundant membrane proteins in CDVs and also show the most difference in expression level between EVs among the tested (Figure 2d), this finding reveals a potentially novel mechanism by which CDVs interact or enter target cells in a highly efficient manner.

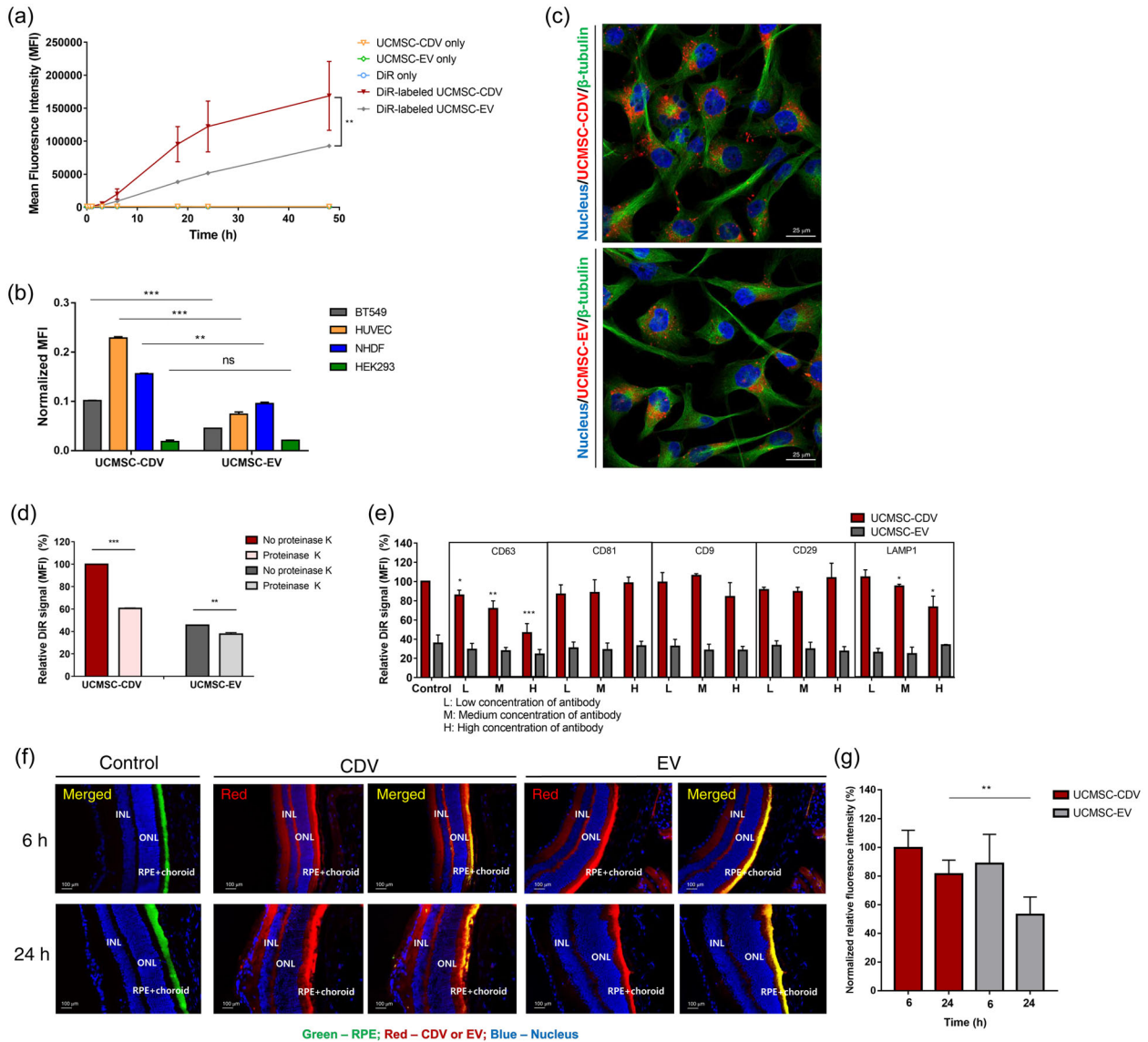


FIGURE 4 Cellular uptake and tissue penetration. (a) Time-dependent cellular uptake of CDVs and EVs was analyzed in BT549 cells by flow cytometry. BT549 cells were seeded on a 24-well plate at 4×10^4 cells/well. The next day, DiR-labelled CDVs (DiR-labelled UCMSC-CDV) and EVs (DiR-labelled UCMSC-EV) were added to the cells at 1×10^5 particles per cell concentration and incubated at 37°C for 1, 3, 6, 18, 24 and 48 h, along with control groups: dye only (DiR only) or unlabelled CDVs (UCMSC-CDV only) or EVs (UCMSC-EV only). After harvesting cells at each time point, the fluorescence intensity was measured using a flow cytometer to determine the uptake efficiency. Data represent the mean \pm SEM from two independent experiments using different batches of CDVs or EVs. The *p*-value was determined by a two-way analysis of variance (ANOVA). $^{**}p < 0.01$. (b) Enhanced CDV uptake was observed from diverse recipient cells. BT549, HUVEC, NHDF and HEK293 cells were used, and the uptake efficiency was analysed 24 h after incubating with UCMSC-CDVs or UCMSC-EVs as described above. All uptake assays were repeated using two different batches of CDVs and EVs. Data represent the mean \pm SD. An unpaired *t*-test was employed. $^{**}p < 0.01$, $^{***}p < 0.001$. ns. Not significant. (c) For confocal microscopy, BT549 cells treated with DiR-UCMSC-CDVs or DiR-UCMSC-EVs, as described above, were collected at 24 h after incubation. Cells were fixed with paraformaldehyde and subjected to immunostaining and confocal imaging. Representative images are shown here. CDVs or EVs are shown in red (DiR); cytoplasm in green (anti- β -tubulin antibody); nucleus in blue (Hoechst counterstain). Scale bar: 25 μm . (d) Digestion (proteinase K) or (e) blockade by antibodies of membrane proteins resulted in a target-specific reduction in cellular uptake. (d) To digest surface proteins, UCMSC-CDVs and UCMSC-EVs were treated with proteinase K at 0.2 μg proteinase K/ μg protein before labelling with DiR. DiR-labelled CDVs and EVs were then added to BT549 cells at 1×10^5 particles per cell concentration and incubated at 37°C for 24 h. (e) For the surface protein blocking, 2×10^9 particles of DiR-labelled CDVs and EVs were treated with antibodies against CD63, CD81, CD9, CD29 and LAMP-1 at 1:100 (high), 1:1000 (medium) or 1:10,000 (low) dilution for 30 min at 4°C in the dark. The fluorescence intensity was measured using a flow cytometer to determine the uptake efficiency. The fluorescence intensity of proteinase K-untreated (d) or antibody-untreated (e) DiR-UCMSC-CDVs was used to normalise each data for comparative analysis. Data represent the mean \pm SD ($N = 2$ for proteinase K; $N = 3$ for antibody blockade). An unpaired *t*-test was employed. $^*p < 0.05$, $^{**}p < 0.01$, $^{***}p < 0.001$. (f) Retinal penetration of CDVs and EVs. A total of 1.5 μl of DiD-labelled UCMSC-CDVs or UCMSC-EVs (approximately 1×10^{11} particles/ml) were injected into the right eye (intravitreal injection) along with PBS control. The mice were sacrificed at 6 and 24 h post injection. The eyeball was removed, fixed in paraformaldehyde, sectioned at 7 μm thickness, and subjected to immunostaining and imaging under the epifluorescence microscope. Representative fluorescence images after 6 and 24 h of intravitreal injection are shown. CDVs or EVs colocalised in the RPE and choroid tissue are shown in bright yellow (Merged, combining red and green channels), while the relative quantity of CDVs or EVs in the retinal tissues can be visualised better without a green channel (Red). Nuclei were stained with DAPI (blue), RPE with anti-RPE65 (green) and CDVs or EVs with DiD (red). ONL (outer nuclear layer); INL (inner nuclear layer); RPE (retinal pigment epithelium). Scale bar: 100 μm . (g) Quantitation results show the relative intensity of the fluorescence signal in the retina normalised by the total input signal. Data represent the mean \pm S.D. An unpaired *t*-test was employed. $^{**}p < 0.01$

The precise route of CDV uptake can be determined by utilising diverse cellular entry pathway blockers. Three well-established uptake inhibitors were used to address this: Dynasore for clathrin-mediated endocytosis; cytochalasin D for actin-dependent phagocytosis and micropinocytosis; heparin for the HSPG receptor-mediated endocytosis. When tested in the BT549 cell line, the uptake of CDVs was suppressed by more than 50% by all three inhibitors at the highest concentration, with cytochalasin D showing the greatest effect among the three (~80% suppression) (Figure S4A). This suggests that the uptake of CDVs occurs via multiple pathways, including dynamin-dependent endocytosis, actin-dependent phagocytosis/micropinocytosis and HSPG receptor-mediated endocytosis. Incubation at 4°C attenuated the CDV uptake significantly compared to 37°C, suggesting an energy-dependent process rather than nonspecific binding (Figure S4B). Furthermore, the degree of inhibition was similar between CDVs and EVs for each inhibitor, compared to their untreated controls, suggesting that both vesicles take similar paths for cellular entry. There is also a possibility that CDVs can enter the cell through yet unidentified or untested routes, requiring further exploration.

Lastly, we challenged the similarly labelled CDVs or EVs in the eye tissue to see how effectively they can cross the retinal tissue barrier. As anticipated, both CDVs and EVs showed excellent penetration into the deep retinal layer upon intravitreal injection, particularly the RPE, which has been implicated in many detrimental human diseases such as age-related macular degeneration (Figure 4f). The quantification results showed slightly higher fluorescence intensity in CDVs compared to EVs, with the difference more prominent after 24 h of injection (Figure 4g). This result suggests that CDVs can serve as an excellent nano-carrier of various drug cargos across the retinal tissue or other tissue barriers, which is subject to further investigation.

3.5 | Biological activity of CDVs

For both CDVs and EVs, the physicochemical characterisation, such as determining the size and number of the vesicles, profiling their protein surface composition and total protein amount, does not reveal information on the biological activity *in vitro* and *in vivo*. Therefore, quality control metrics to measure not only key identity but also activity features of CDVs have to be specified. Critical Quality Attributes (CQA) are commonly chosen based on the established or hypothesised mode of action of a substance related to certain bioactivity in a specific disease (Demmon et al., 2020). For UCMSC-CDVs and UCMSC-EVs, the mode of action is not clearly defined. However, information on the biological activity of a stable component can provide valuable information on the overall stability of the product as well as on the potential alterations upon prolonged storage.

One biological activity that can be generally attributed to both EVs and CDVs is immunomodulation. Combining cell-based (induced T-cell proliferation) and biochemical assays (CD73 enzymatic activity), we show that CDVs display biological activity comparable to that reported previously for well-characterised UCMSC-EVs. The immunomodulation assay using pooled human PBMC-derived T-cells reveals that CDVs from several individual batches all display considerable levels of immunomodulatory activities, ranging from 16% to 38% inhibition (Figure 5a). It must be acknowledged, however, that a cell-based assay such as the one described here suffers from significant variability between PBMC batches and that the inhibition of induced T-cell proliferation cannot be quantified with sufficient precision (Kordelas et al., 2019).

Adenosine signalling via the enzymatic activity of GPI-anchored ecto-5'-nucleotidase CD73/NT5E may also contribute to the biological activity in a decisive manner. We have previously shown that CD73 is present on UCMSC-EVs and that UCMSC-EV preparations actively converted adenosine monophosphate (AMP) in a biochemical assay in a dose-dependent manner (Priglinger et al., 2021). CD73 is a well-known plasma membrane-anchored surface marker for cultured MSCs in mice and humans. UCMSCs thus display significant amounts of CD73 in the plasma membrane and the enzyme is retained on the surface of UCMSC-CDVs. All CDV preparations displayed a considerable activity of AMP consumption and average activity values were determined to be 5.96×10^{-8} μM adenosine production per CDV particle (Figure 5b).

Lastly, the inflammatory response is largely controlled by cytokines which induce an acute phase response to protect the host against irritation, injury and infection. Cytokines are critical mediators of immune and inflammatory responses via complex networks and quantification of cytokines has significant value for pre-clinical and clinical investigation. Pro-inflammatory cytokines include IL-1, IL-6, IL-8, IL-12, IL-18, IFN- γ and TNF- α . The major role of these cytokines is to communicate with surrounding tissue-resident cells, leading to immune cell activation and significant alteration in host physiology (Liu et al., 2021). Preparations that are intended to induce immunosuppressive or immunomodulatory activities should thus contain low levels of pro-inflammatory cytokines to avoid activities that could influence the outcome of *in vivo* experiments. Using the MSD solid phase system that can detect ultralow levels of human pro-inflammatory cytokines, we found that UCMSC-CDVs contain very low levels (below ~2 pg/ml) of pro-inflammatory cytokines with only IL-6 (ranging from 4 to 49 pg/ml) and IL-8 (from 17 to 145 pg/ml) being detectable reliably (Figure 5c).

3.6 | Establishment of GMP-compliant manufacturing process

Finally, the process of CDV manufacturing via extrusion was successfully adapted to the general current GMP (cGMP) requirements and conditions for operation in a class B cleanroom environment. We have previously reported EV manufacturing in the

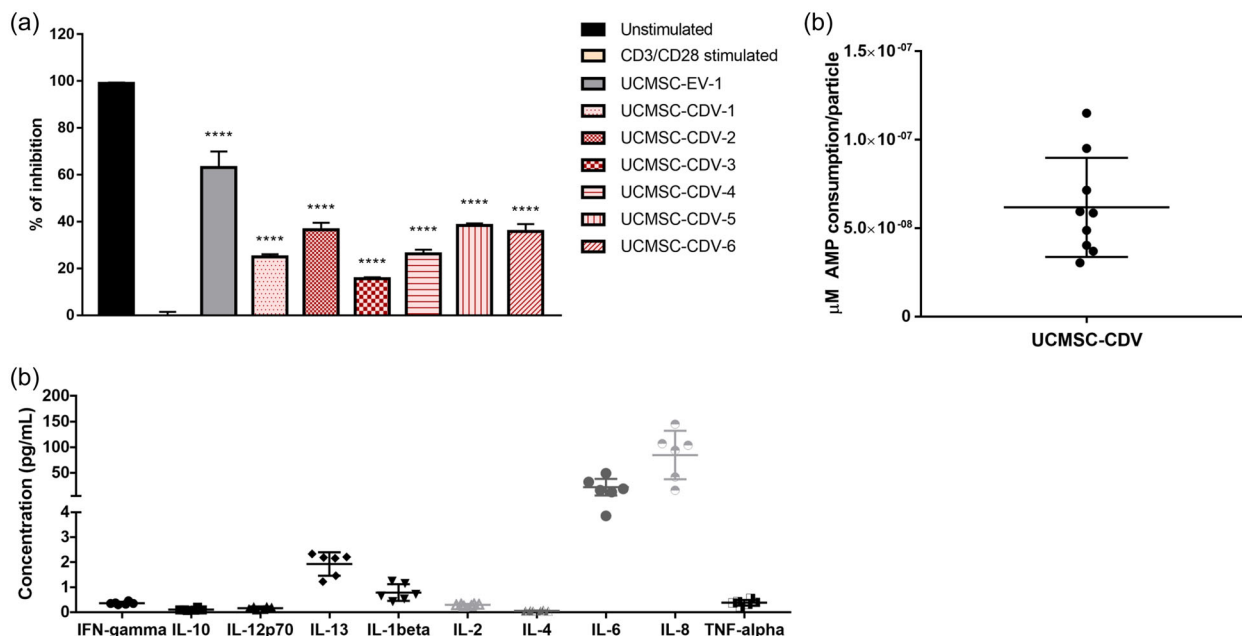


FIGURE 5 Biological activity of CDVs. (a) The immunomodulation activity of CDVs and EVs was assessed in an in vitro T-cell proliferation assay. CFSE-pre-labelled human PBMCs were stimulated with CD3/CD28 and co-cultured with UCMSC-CDVs or UCMSC-EVs for 72 h at a ratio of $0.5\text{--}1 \times 10^4$ particles per cell (3×10^5 cells per assay). Six different batches of CDVs produced in independent production runs (denoted as UCMSC-CDV-1 to -6) were used in comparison with a single batch of EVs (denoted as UCMSC-EV-1). The percentage of inhibition of T-cell proliferation was analyzed by flow cytometer ($N = 3$). Data represent the mean \pm SD. An unpaired *t*-test was employed. **** $p < 0.0001$. (b) The CD73 activity of CDVs was determined using the AMP-Glo Assay kit. A total of $10 \mu\text{l}$ of CDVs (approximately $3 \times 10^8\text{--}3 \times 10^9$ particles) from nine different production batches were incubated with $10 \mu\text{M}$ AMP for 20 min at 37°C , and the enzymatic activity (conversion of AMP to adenosine) was measured by AMP-Glo Assay kit. Data represent the mean \pm SD. (c) Pro-inflammatory cytokine profiles were obtained from six different batches of UCMSC-CDVs using the V-Plex and U-Plex human multiplex immunoassay kits. Data represent the mean \pm SD

same cGMP environment and successfully applied it to human patients (Gimona et al., 2017; Rohde et al., 2019; Warnecke et al., 2021). Many process development components were shared between EVs and CDVs, except that the development of a disposable centre unit of ES50 to replace the metal parts was necessary (Figure S5). Process and quality control parameters for the manufacturing process of UCMSC-CDVs were established, including the documentation of all cell expansion and extrusion processes and the creation of standard operating procedures (SOPs), standard forms, checklists and acceptance criteria (Table 1).

Results from individual training runs revealed that the overall process design and the developed SOPs were suitable for executing the manufacturing of UCMSC-CDVs with high batch-to-batch consistency. Key acceptance criteria are summarised in Table 1. These include a panel of identity measures: particle size; particle yield per cell; protein amount; residual amounts of DNA and benzonase; surface marker profile of up to six key molecules, consisting of CD9, CD63, CD81 (canonical EV markers), CD29, CD90 (abundant in CDVs) and CD73 (abundant in CDVs, potency marker); as well as representative marker profile of producer cells, UCMSC, at time of harvest. Please note that CD73 and CD90 are not included in the standard MACSPlex kit and the presence of these two markers is thus manually determined by adding the respective antibodies to the MACSPlex kit (see Section 2.6; Figure S6). The safety of CDVs was measured using methods widely used in the quality control of biological products such as endotoxin and mycoplasma levels and sterility. To further control the potential for batch-to-batch variations among CDV preparations, we have established Master and Working Cell banks from a tested primary umbilical cord-derived MSC population as previously described (Pachler, Ketterl, et al., 2017; Priglinger et al., 2021). Both banks were tested for the presence of human pathogenic virus and mycoplasma as well as for sterility according to Pharm. Eur. (Virusure, Austria). All GMP-compliant CDV batches were tested for endotoxin levels and sterility (AGES Graz, Austria), and mycoplasma levels were determined according to Pharm. Eur. in certified laboratories (EUROFINS, Italy). Finally, the potency was determined by the enzymatic activity of CD73. Adhering to the established SOPs, CDV batches were manufactured that met all the acceptance criteria as shown below in Table 1.

4 | DISCUSSION

Compared to the EVs with relatively well-characterised biogenesis, limited studies were conducted to unveil the formation of CDVs. It is widely documented that EVs are formed by the inward budding and multivesicular bodies, followed by the

maturation of endosomes. The matured endosomes are then naturally released from the cells via exocytosis, likely via the lipid raft of the microdomain in the plasma membrane (Bonifacino & Glick, 2004; Kalluri & LeBleu, 2020; They et al., 2002), thus contain relatively low subcellular organelle proteins. In contrast, CDVs are produced from the extrusion of cells, which appears to result in the use of rich lipid sources of cells, including subcellular organelle membranes in addition to the plasma membranes. Although a typical cell consists of nearly 10%–15% of the phospholipid distribution in the plasma membrane (Escriba et al., 2015), the remaining 85%–90% of phospholipids can be found in the subcellular organelle membranes. Our data demonstrate this by showing the enrichment of membrane proteins, characteristic of major subcellular organelles such as ER, Golgi apparatus, lysosome and possibly many other intracellular vesicles (Figure 2d). Interestingly, the expression patterns of well-known tetraspanin markers, such as CD9, CD63 and CD81, are considerably different between CDVs and EVs, reflecting the difference in their origin or mechanism of production (Figure 2d). These data support the hypothesis that CDVs are composed of diverse membrane sources of parent cells and reveal the possible mechanism by which superior yield is obtained using extrusion technology (Figure 3g). Despite the diverse composition of CDV membrane due to the diverse origin, CDVs showed comparable or even enhanced cellular uptake or tissue penetration capability in multiple target cells compared to EVs, promoting their potential as efficient drug delivery systems to various compartments or cellular targets (Figure 4).

MSCs have been widely studied as potential cell therapy candidates for various diseases, mainly to repair damaged tissues due to their regenerative capacity. Despite the advantages of MSCs as a cell therapy agent, there exist multiple concerns regarding their safety and therapeutic potency and clinical challenges that need to be considered (Levy et al., 2020; Wang et al., 2021). MSC transplantation may form a tumour due to its reproductive capacity and promote the tumour environment by modulating the immune system (Barkholt et al., 2013; Neri, 2019). Multiple studies reported that administered MSCs may cause pulmonary embolism due to cell accumulation or thrombus formation (Tatsumi et al., 2013; Wu et al., 2017). Also, due to the character of the cells, the mode of administration can be critical to maintaining the efficacy of the treatment, for example, injection device needle size and pressure (Levy et al., 2020). MSC-derived CDVs may serve as an excellent alternative to MSCs without posing those risks. CDVs can not only eliminate the risk of tumour formation or cell aggregation but also simplify the handling and administration regimen of the treatment. Furthermore, CDVs can penetrate through diverse cellular and tissue barriers that cells cannot cross as shown above (Figure 4). With diverse technologies to engineer CDVs available, it is also plausible to achieve target-selective delivery.

The presence of class I human leucocyte antigens (HLA) on the surface of CDVs raises concerns about the possibility of inducing a donor-specific immune response in patients receiving CDVs derived from allogeneic UCMSCs. Thus, the safety profile of UCMSC-CDVs must be evaluated prior to any future clinical application. Notably, however, a low expression level of HLA-I antigens seems to mediate the escape of MSCs from the recipient's immunological surveillance (Wang et al., 2019). Moreover, works from Bartolucci et al. (2017) and Sanabria-de la Torre et al. (2021) confirm the absence of humoral immune reaction to transplanted or infused UCMSCs and that UCMSCs do not induce alloantigen-directed antibodies in patients (Bartolucci et al., 2017; Sanabria-de la Torre et al., 2021). Together, these findings suggest that UCMSC-CDVs are safe with regard to the presence of HLA-I antigens and that the possibility for the generation of alloantibodies is of limited clinical relevance. In agreement with our previous work on UCMSC-EVs (Warnecke et al., 2020), we detected the presence of pro-inflammatory cytokines in various CDV batches to reside in the low pg/mL range. Except for IL-6 and IL-8, the levels of all other tested pro-inflammatory cytokines were close to or below the detection limit of the assay system. These findings add to the overall positive safety profile of UCMSC-CDVs. In addition, multiple attempts to evaluate the toxicity and immunogenicity of CDVs show that the safety risks associated with CDVs are low: a GLP-Tox study was conducted using human NK cell-derived CDVs. Upon multiple dosing of NK-CDVs in rodents, no CDV-specific safety concerns were detected (data not shown); mixed lymphocyte reaction (MLR) assay using UCMSC-CDVs and human PBMCs also revealed that the immunogenicity of CDVs is low when compared to allogeneic PBMCs or other standard controls (data not shown). CDVs derived from other cell types also showed that there are no noticeable safety concerns thus far (data not shown). Clearly, continuous and rigorous monitoring of all safety-related parameters must be conducted prior to clinical testing on humans.

While understanding the precise mechanism underlying the biological activities exerted by CDVs requires extensive additional investigation, we found that the common immunomodulatory capacity observed in multiple studies of MSC-derived EVs exists in UCMSC-CDVs. One of the widely-used cellular assays testing the immunomodulatory effect of EVs analyses the proliferation activity of T-cells upon stimulation with mitogens, such as Concanavalin A (Yeo et al., 2013) or phytohemagglutinin (Pachler, Ketterl, et al., 2017), anti-CD3/CD28 beads (Trickett & Kwan, 2003) or by mixing lymphocytes from multiple donors to induce MLR (Ketterl et al., 2015), with or without testing reagents. However, the results comparing the immunomodulatory potential of MSC-EVs and the cellular source MSCs have been controversial among multiple studies. Several studies reported that MSCs-EVs failed to present the immunomodulatory effect of MSCs (Conforti et al., 2014; Di Trapani et al., 2016; Gouveia de Andrade et al., 2015), while others (Pachler, Ketterl, et al., 2017; Yeo et al., 2013) presented data demonstrating the competency of MSC-EVs in inhibiting lymphocyte proliferation, consistent with our results (Figure 5a). In searching for the likely explanation of these discrepancies, it is worth considering the potential drawbacks of naturally secreted EVs, for instance, extremely low production yield and difficulties in standardisation in small-scale research. In addition, CD73 activity has been implicated in the immunomodulatory potential of MSC-EVs. CD73 is an ecto-5'-nucleotidase residing on the plasma membrane that converts

extracellular AMP to adenosine, which is a key immunosuppressive metabolite limiting immune responses in multiple tissues (Arslan et al., 2013; Chew et al., 2019; Lai et al., 2013; Zhai et al., 2021; Zhang et al., 2018). Albeit very rare in humans, CD73 is also involved in a genetic disorder, in which patients present the complex phenotype of arterial calcification due to a deficiency of CD73 (ACDC) (Joolharzadeh & St Hilaire, 2019; St Hilaire et al., 2011). As genetic rescue or supplementation of adenosine reduces the severity of calcification, CDVs also hold the considerable therapeutic potential to this end.

Presently, only a few clinical validation studies and defined manufacturing processes exist for cell-derived vesicular biopharmaceutical candidates such as EVs. Yet, this rapidly expanding field requires the definition of a standardised and reproducible engineering basis for production early in the development cycle to ensure cost-effective manufacturing at the appropriate scale (Colao et al., 2018). Thus, the effective translation of vesicle-based biotherapeutics into the clinic requires scalable manufacturing processes that fulfil the requirements of GMP (Staubach et al., 2021). Despite the biological and regulatory complexity of the field, we have attempted the development of scalable and reproducible purification protocols for UCMSC-CDVs based on robust risk-based approaches, and to elucidate various mechanisms of action through qualified potency assays in disease-relevant models as previously described (Rohde et al., 2019). Importantly, we have successfully transferred our research scale manufacturing process for CDVs into SOP-guided GMP-compliant processes that give rise to products with high batch-to-batch consistency. We have also capitalised on the experience made with the GMP-compliant manufacturing of secreted EVs for clinical testing that relies on the enrichment of cellular vesicles by serial filtration based on the scalable technology of TFF in the downstream (purification) part (Warnecke et al., 2020). The overall GMP compliance of our manufacturing process and the use of fully tested Master and Working Cell banks for the upstream (cell expansion) process allows for a more rapid clinical testing of the biologically and, expectedly, also therapeutically active UCMSC-CDVs in humans. In addition, the inherent possibility to load the CDVs with therapeutically active compounds, such as mRNAs or small RNAs (e.g., miRNAs), in a cleanroom environment following the same SOP-guided process extends the possibilities for future therapeutic product development based on the CDV technology.

CDVs and other related EV-mimetic nanovesicles increasingly challenge the preferred use of EVs as many of the multidimensional biological effects of EVs are well-preserved in CDVs. Besides the well-described advantage in productivity, the CDV technology also eliminates several variabilities brought about by the poorly understood and environment-sensitive biogenesis of EVs, and positions CDVs as a unique and versatile biological medicinal product for application as both a therapeutic and drug delivery system.

AUTHOR CONTRIBUTIONS

Hui-Chong Lau: Methodology, Investigation, Data analysis, Data curation, Manuscript writing; Dong Woo Han and Jinhee Park: Methodology, Investigation, Data analysis, Data curation; Edwine Lehner, Carina Kals, Claudia Arzt, Elisabeth Bayer, Daniela Auer, Tanja Schally, Eva Grasmann and Han Fang: Methodology, Investigation (GMP lab), Data analysis, Data curation; Jae-Young Lee and Hyun Soo Lee: Investigation (retinal penetration), Data analysis, Data curation; Jinah Han: Manuscript writing & editing; Mario Gimona: Methodology, Project administration, Supervision (GMP lab), Manuscript writing & review; Eva Rohde: Project administration, Supervision (GMP lab); Shingyu Bae: Conceptualization, Resources, Project administration; Seung Wook Oh: Conceptualization; Supervision, Project administration, Data curation, Manuscript writing, editing & review. All authors read, edited and approved the final manuscript.

ACKNOWLEDGEMENTS

We are grateful for all the advice, support and encouragement from advisors, investors and staff members of MDimune Inc. MG gratefully acknowledges the financial support by P1812596 'EV-TT' (Land Salzburg/IWB/EFRE) and 20102-F1900731-KZP 'EV-TT – Bpro' (Land Salzburg/WISS 2025).

CONFLICT OF INTEREST

MG receives financial support from MDimune for consulting activities. ER had received compensation from MDimune for consulting activities as a medical advisor (2020–2021). The authors have no other disclosure.

ORCID

Seung Wook Oh  <https://orcid.org/0000-0001-7632-6822>

REFERENCES

- Arslan, F., Lai, R. C., Smeets, M. B., Akeroyd, L., Choo, A., Aguar, E. N. E., Timmers, L., Van Rijen, H. V., Doevendans, P. A., Pasterkamp, G., Lim, S. K., & De Kleijn, D. P. (2013). Mesenchymal stem cell-derived exosomes increase ATP levels, decrease oxidative stress and activate PI3K/Akt pathway to enhance myocardial viability and prevent adverse remodeling after myocardial ischemia/reperfusion injury. *Stem Cell Research*, 10, 301–312.
- Barilani, M., Peli, V., Cherubini, A., Dossena, M., Dolo, V., & Lazzari, L. (2019). NG2 as an identity and quality marker of mesenchymal stem cell extracellular vesicles. *Cells*, 8, 1524.
- Barkholt, L., Flory, E., Jekerle, V., Lucas-Samuel, S., Ahnert, P., Bisset, L., Büscher, D., Fibbe, W., Foussat, A., Kwa, M., Lantz, O., Mačulaitis, R., Palomäki, T., Schneider, C. K., Sensebé, L., Tachdjian, G., Tarte, K., Tosca, L., & Salmikangas, P. (2013). Risk of tumorigenicity in mesenchymal stromal cell-based therapies—bridging scientific observations and regulatory viewpoints. *Cytotherapy*, 15, 753–759.

- Bartolucci, J., Verdugo, F. J., Gonzalez, P. L., Larrea, R. E., Abarzua, E., Goset, C., Rojo, P., Palma, I., Lamich, R., Pedreros, P. A., Valdivia, G., Lopez, V. M., Nazzal, C., Alcayaga-Miranda, F., Cuenca, J., Brobeck, M. J., Patel, A. N., Figueroa, F. E., & Khoury, M. (2017). Safety and efficacy of the intravenous infusion of umbilical cord mesenchymal stem cells in patients with heart failure: A phase 1/2 randomized controlled trial (RIMECARD Trial [Randomized Clinical Trial of Intravenous Infusion Umbilical Cord Mesenchymal Stem Cells on Cardiopathy]). *Circulation Research*, *121*, 1192–1204.
- Bonifacino, J. S., & Glick, B. S. (2004). The mechanisms of vesicle budding and fusion. *Cell*, *116*, 153–166.
- Cardoso, R. M. S., Rodrigues, S. C., Gomes, C. F., Duarte, F. V., Romao, M., Leal, E. C., Freire, P. C., Neves, R., & Simões-Correia, J. (2021). Development of an optimized and scalable method for isolation of umbilical cord blood-derived small extracellular vesicles for future clinical use. *Stem Cells Translational Medicine*, *10*, 910–921.
- Chew, J. R. J., Chuah, S. J., Teo, K. Y. W., Zhang, S., Lai, R. C., Fu, J. H., Lim, L. P., Lim, S. K., & Toh, W. S. (2019). Mesenchymal stem cell exosomes enhance periodontal ligament cell functions and promote periodontal regeneration. *Acta Biomaterialia*, *89*, 252–264.
- Choo, Y. W., Kang, M., Kim, H. Y., Han, J., Kang, S., Lee, J. R., Jeong, G. J., Kwon, S. P., Song, S. Y., Go, S., Jung, M., Hong, J., & Kim, B. S. (2018). M1 macrophage-derived nanovesicles potentiate the anticancer efficacy of immune checkpoint inhibitors. *ACS Nano*, *12*, 8977–8993.
- Colao, I. L., Corteling, R., Bracewell, D., & Wall, I. (2018). Manufacturing exosomes: A promising therapeutic platform. *Trends in Molecular Medicine*, *24*, 242–256.
- Conforti, A., Scarsella, M., Starc, N., Giorda, E., Biagini, S., Proia, A., Carsetti, R., Locatelli, F., & Bernardo, M. E. (2014). Microvesicles derived from mesenchymal stromal cells are not as effective as their cellular counterpart in the ability to modulate immune responses in vitro. *Stem Cells and Development*, *23*, 2591–2599.
- Cvjetkovic, A., Jang, S. C., Konečná, B., Höög, J. L., Sihlbom, C., Lässer, C., & Lötvall, J. (2016). Detailed analysis of protein topology of extracellular vesicles—evidence of unconventional membrane protein orientation. *Scientific Reports*, *6*, 36338.
- Demmon, S., Bhargava, S., Ciolek, D., Halley, J., Jaya, N., Joubert, M. K., Koepf, E., Smith, P., Trexler-Schmidt, M., & Tsai, P. (2020). A cross-industry forum on benchmarking critical quality attribute identification and linkage to process characterization studies. *Biologicals: journal of the International Association of Biological Standardization*, *67*, 9–20.
- Desgeorges, A., Hollerweger, J., Lassacher, T., Rohde, E., Helmbrecht, C., & Gimona, M. (2020). Differential fluorescence nanoparticle tracking analysis for enumeration of the extracellular vesicle content in mixed particulate solutions. *Methods (San Diego, Calif.)*, *177*, 67–73.
- Di Trapani, M., Bassi, G., Midolo, M., Gatti, A., Takam Kanga, P., Cassaro, A., Carusone, R., Adamo, A., & Krampera, M. (2016). Differential and transferable modulatory effects of mesenchymal stromal cell-derived extracellular vesicles on T, B and NK cell functions. *Scientific Reports*, *6*, 24120.
- Dominici, M., Le Blanc, K., Mueller, I., Slaper-Cortenbach, I., Marini, F. C., Krause, D. S., Deans, R. J., Keating, A., Prockop, D. J., & Horwitz, E. M. (2006). Minimal criteria for defining multipotent mesenchymal stromal cells. The International Society for Cellular Therapy position statement. *Cytherapy*, *8*, 315–317.
- Dooley, K., Mcconnell, R. E., Xu, K., Lewis, N. D., Haupt, S., Youniss, M. R., Martin, S., Sia, C. L., McCoy, C., Moniz, R. J., Burenkova, O., Sanchez-Salazar, J., Jang, S. C., Choi, B., Harrison, R. A., Houde, D., Burzyn, D., Leng, C., Kirwin, K., ... Williams, D. E. (2021). A versatile platform for generating engineered extracellular vesicles with defined therapeutic properties. *Molecular Therapy*, *29*, 1729–1743.
- Emelyanov, A., Shtam, T., Kamyshinsky, R., Garaeva, L., Verlov, N., Miliukhina, I., Kudrevatykh, A., Gavrilov, G., Zabrodskaia, Y., Pchelina, S., & Konevega, A. (2020). Cryo-electron microscopy of extracellular vesicles from cerebrospinal fluid. *PLoS ONE*, *15*, e0227949.
- Escribá, P. V., Busquets, X., Inokuchi, J. I., Balogh, G., Török, Z., Horváth, I., Harwood, J. L., & Vigh, L. (2015). Membrane lipid therapy: Modulation of the cell membrane composition and structure as a molecular base for drug discovery and new disease treatment. *Progress in Lipid Research*, *59*, 38–53.
- Gimona, M., Pachler, K., Laner-Plamberger, S., Schallmoser, K., & Rohde, E. (2017). Manufacturing of human extracellular vesicle-based therapeutics for clinical use. *International Journal of Molecular Sciences*, *18*, 1190.
- Goh, W. J., Lee, C. K., Zou, S., Woon, E., Czarny, B., & Pastorin, G. (2017). Doxorubicin-loaded cell-derived nanovesicles: An alternative targeted approach for anti-tumor therapy. *International Journal of Nanomedicine*, *12*, 2759–2767.
- Goh, W. J., Zou, S., Ong, W. Y., Torta, F., Alexandra, A. F., Schiffelers, R. M., Storm, G., Wang, J. W., Czarny, B., & Pastorin, G. (2017). Bioinspired cell-derived nanovesicles versus exosomes as drug delivery systems: A cost-effective alternative. *Scientific Reports*, *7*, 14322.
- Gouveia De Andrade, A. V., Bertolino, G., Riewaldt, J., Bieback, K., Karbanová, J., Odendahl, M., Bornhäuser, M., Schmitz, M., Corbeil, D., & Tonn, T. (2015). Extracellular vesicles secreted by bone marrow- and adipose tissue-derived mesenchymal stromal cells fail to suppress lymphocyte proliferation. *Stem Cells and Development*, *24*, 1374–1376.
- Hong, J., Kang, M., Jung, M., Lee, Y. Y., Cho, Y., Kim, C., Song, S. Y., Park, C. G., Doh, J., & Kim, B. S. (2021). T-cell-derived nanovesicles for cancer immunotherapy. *Advanced Materials*, *33*, 2101110.
- Jang, S. C., Kim, O. Y., Yoon, C. M., Choi, D. S., Roh, T. Y., Park, J., Nilsson, J., Lötvall, J., Kim, Y. K., & Gho, Y. S. (2013). Bioinspired exosome-mimetic nanovesicles for targeted delivery of chemotherapeutics to malignant tumors. *ACS Nano*, *7*, 7698–7710.
- Joolharzadeh, P., & St Hilaire, C. (2019). CD73 (Cluster of Differentiation 73) and the differences between mice and humans. *Arteriosclerosis, Thrombosis, and Vascular Biology*, *39*, 339–348.
- Kalimuthu, S., Gangadaran, P., Rajendran, R. L., Zhu, L., Oh, J. M., Lee, H. W., Gopal, A., Baek, S. H., Jeong, S. Y., Lee, S. W., Lee, J., & Ahn, B. C. (2018). A new approach for loading anticancer drugs into mesenchymal stem cell-derived exosome mimetics for cancer therapy. *Frontiers in Pharmacology*, *9*, 1116.
- Kalluri, R., & Lebleu, V. S. (2020). The biology, function, and biomedical applications of exosomes. *Science*, *367*, eaau6977.
- Ketterl, N., Brachtel, G., Schuh, C., Bieback, K., Schallmoser, K., Reinisch, A., & Strunk, D. (2015). A robust potency assay highlights significant donor variation of human mesenchymal stem/progenitor cell immune modulatory capacity and extended radio-resistance. *Stem Cell Research & Therapy*, *6*, 236.
- Kim, H. Y., Kumar, H., Jo, M. J., Kim, J., Yoon, J. K., Lee, J. R., Kang, M., Choo, Y. W., Song, S. Y., Kwon, S. P., Hyeon, T., Han, I. B., & Kim, B. S. (2018). Therapeutic efficacy-potentiated and diseased organ-targeting nanovesicles derived from mesenchymal stem cells for spinal cord injury treatment. *Nano Letters*, *18*, 4965–4975.
- Kim, Y. S., Kim, J. Y., Cho, R., Shin, D. M., Lee, S. W., & Oh, Y. M. (2017). Adipose stem cell-derived nanovesicles inhibit emphysema primarily via an FGF2-dependent pathway. *Experimental & Molecular Medicine*, *49*, e284.
- Ko, K. W., Yoo, Y. I., Kim, J. Y., Choi, B., Park, S. B., Park, W., Rhim, W. K., & Han, D. K. (2020). Attenuation of tumor necrosis factor-alpha induced inflammation by umbilical cord-mesenchymal stem cell derived exosome-mimetic nanovesicles in endothelial cells. *Journal of Tissue Engineering and Regenerative Medicine*, *17*, 155–163.
- Kordelas, L., Schwich, E., Dittrich, R., Horn, P., Beelen, D., Börger, V., Giebel, B., & Rebmann, V. (2019). Individual immune-modulatory capabilities of MSC-derived extracellular vesicle (EV) preparations and recipient-dependent responsiveness. *International Journal of Molecular Sciences*, *20*, 1642.
- Kwon, M. H., Song, K. M., Limanjaya, A., Choi, M. J., Ghatak, K., Nguyen, N. M., Ock, J., Yin, G. N., Kang, J. H., Lee, M. R., Gho, Y. S., Ryu, J. K., & Suh, J. K. (2019). Embryonic stem cell-derived extracellular vesicle-mimetic nanovesicles rescue erectile function by enhancing penile neurovascular regeneration in the streptozotocin-induced diabetic mouse. *Scientific Reports*, *9*, 20072.

- Laner-Plamberger, S., Lener, T., Schmid, D., Streif, D. A., Salzer, T., Öller, M., Hauser-Kronberger, C., Fischer, T., Jacobs, V. R., Schallmoser, K., Gimona, M., & Rohde, E. (2015). Mechanical fibrinogen-depletion supports heparin-free mesenchymal stem cell propagation in human platelet lysate. *Journal of Translational Medicine*, 13, 354.
- Lee, H., Kang, H., Kang, M., Han, C., Yi, J., Kwon, Y., & Park, J. (2020). Heterogeneous subcellular origin of exosome-mimetic nanovesicles engineered from cells. *ACS Biomaterials Science & Engineering*, 6, 6063–6068.
- Lee, J. R., Kyung, J. W., Kumar, H., Kwon, S. P., Song, S. Y., Han, I. B., & Kim, B. S. (2020). Targeted delivery of mesenchymal stem cell-derived nanovesicles for spinal cord injury treatment. *International Journal of Molecular Sciences*, 21, 4185.
- Levy, O., Kuai, R., Siren, E. M. J., Bhere, D., Milton, Y., Nissar, N., De Biasio, M., Heinelt, M., Reeve, B., Abdi, R., Alturki, M., Fallatah, M., Almalik, A., Alhasan, A. H., Shah, K., & Karp, J. M. (2020). Shattering barriers toward clinically meaningful MSC therapies. *Science Advances*, 6, eaba6884.
- Li, Y. J., Wu, J. Y., Liu, J., Xu, W., Qiu, X., Huang, S., Hu, X. B., & Xiang, D. X. (2021). Artificial exosomes for translational nanomedicine. *Journal of Nanobiotechnology*, 19, 242.
- Liu, C., Chu, D., Kalantar-Zadeh, K., George, J., Young, H. A., & Liu, G. (2021). Cytokines: From clinical significance to quantification. *Advanced Science (Weinheim)*, 8, 2004433.
- Lunavat, T. R., Jang, S. C., Nilsson, L., Park, H. T., Repiska, G., Lässer, C., Nilsson, J. A., Gho, Y. S., & Lötvall, J. (2016). RNAi delivery by exosome-mimetic nanovesicles - Implications for targeting c-Myc in cancer. *Biomaterials*, 102, 231–238.
- Nasiri Kenari, A., Cheng, L., & Hill, A. F. (2020). Methods for loading therapeutics into extracellular vesicles and generating extracellular vesicles mimetic-nanovesicles. *Methods (San Diego, Calif.)*, 177, 103–113.
- Nasiri Kenari, A., Kastaniegaard, K., Greening, D. W., Shambrook, M., Stensballe, A., Cheng, L., & Hill, A. F. (2019). Proteomic and post-translational modification profiling of exosome-mimetic nanovesicles compared to exosomes. *Proteomics*, 19, 1800161.
- Neri, S. (2019). Genetic stability of mesenchymal stromal cells for regenerative medicine applications: A fundamental biosafety aspect. *International Journal of Molecular Sciences*, 20, 2406.
- Pachler, K., Ketterl, N., Desgeorges, A., Dunai, Z., Laner-Plamberger, S., Streif, D., Strunk, D., Rohde, E., & Gimona, M. (2017a). An in vitro potency assay for monitoring the immunomodulatory potential of stromal cell-derived extracellular vesicles. *International Journal of Molecular Sciences*, 18, 1413.
- Pachler, K., Lener, T., Streif, D., Dunai, Z. A., Desgeorges, A., Feichtner, M., Öller, M., Schallmoser, K., Rohde, E., & Gimona, M. (2017b). A good manufacturing practice-grade standard protocol for exclusively human mesenchymal stromal cell-derived extracellular vesicles. *Cytotherapy*, 19, 458–472.
- Park, K. S., Svennerholm, K., Shelke, G. V., Bandeira, E., Lässer, C., Jang, S. C., Chandode, R., Gribonika, I., & Lötvall, J. (2019). Mesenchymal stromal cell-derived nanovesicles ameliorate bacterial outer membrane vesicle-induced sepsis via IL-10. *Stem Cell Research & Therapy*, 10, 231.
- Petrenko, Y., Vackova, I., Kekulova, K., Chudickova, M., Koci, Z., Turnovcova, K., Kupcova Skalnikova, H., Vodicka, P., & Kubinova, S. (2020). A comparative analysis of multipotent mesenchymal stromal cells derived from different sources, with a focus on neuroregenerative potential. *Scientific Reports*, 10, 4290.
- Priglinger, E., Strasser, J., Buchroithner, B., Weber, F., Wolbank, S., Auer, D., Grasmann, E., Arzt, C., Sivun, D., Grillari, J., Jacak, J., Preiner, J., & Gimona, M. (2021). Label-free characterization of an extracellular vesicle-based therapeutic. *Journal of Extracellular Vesicles*, 10, e12156.
- Rohde, E., Pachler, K., & Gimona, M. (2019). Manufacturing and characterization of extracellular vesicles from umbilical cord-derived mesenchymal stromal cells for clinical testing. *Cytotherapy*, 21, 581–592.
- Lai, R. C., Y. R. W. Y., Tan, S. S., Zhang, B., Yin, Y., Sze, N. S. K., Choo, A., & Lim, S. K. (2013). Mesenchymal stem cell exosomes: The future MSC-based therapy? In L. Chase, & M. Vemuri (Eds.), *Mesenchymal stem cell therapy. Stem cell biology and regenerative medicine*. Humana Press.
- Sanabria-De La Torre, R., Quinones-Vico, M. I., Fernandez-Gonzalez, A., Sanchez-Diaz, M., Montero-Vilchez, T., Sierra-Sanchez, A. L., & Arias-Santiago, S. (2021). Alloreactive immune response associated to human mesenchymal stromal cells treatment: A systematic review. *Journal of Clinical Medicine*, 10, 2991.
- St Hilaire, C., Ziegler, S. G., Markello, T. C., Brusco, A., Groden, C., Gill, F., Carlson-Donohoe, H., Lederman, R. J., Chen, M. Y., Yang, D., Siegenthaler, M. P., Arduino, C., Mancini, C., Freudenthal, B., Stanescu, H. C., Zdebik, A. A., Chaganti, R. K., Nussbaum, R. L., Kleta, R., ... Gahl, W. A. (2011). NT5E mutations and arterial calcifications. *New England Journal of Medicine*, 364, 432–442.
- Staubach, S., Bauer, F. N., Tertel, T., Börger, V., Stambouli, O., Salzig, D., & Giebel, B. (2021). Scaled preparation of extracellular vesicles from conditioned media. *Advanced Drug Delivery Reviews*, 177, 113940.
- Tatsumi, K., Ohashi, K., Matsubara, Y., Kohori, A., Ohno, T., Kakidachi, H., Horii, A., Kanegae, K., Utoh, R., Iwata, T., & Okano, T. (2013). Tissue factor triggers procoagulation in transplanted mesenchymal stem cells leading to thromboembolism. *Biochemical and Biophysical Research Communications*, 431, 203–209.
- Thery, C., Zitvogel, L., & Amigorena, S. (2002). Exosomes: Composition, biogenesis and function. *Nature Reviews Immunology*, 2, 569–579.
- Trickett, A., & Kwan, Y. L. (2003). T cell stimulation and expansion using anti-CD3/CD28 beads. *Journal of Immunological Methods*, 275, 251–255.
- Wang, Y., Huang, J., Gong, L., Yu, D., An, C., Bunpetch, V., Dai, J., Huang, H., Zou, X., Ouyang, H., & Liu, H. (2019). The plasticity of mesenchymal stem cells in regulating surface HLA-I. *Science*, 15, 66–78.
- Wang, Y., Yi, H., & Song, Y. (2021). The safety of MSC therapy over the past 15 years: A meta-analysis. *Stem Cell Research & Therapy*, 12, 545.
- Warnecke, A., Harre, J., Staecker, H., Prenzler, N., Strunk, D., Couillard-Despres, S., Romanelli, P., Hollerweger, J., Lassacher, T., Auer, D., Pachler, K., Wietzorrek, G., Köhl, U., Lenarz, T., Schallmoser, K., Laner-Plamberger, S., Falk, C. S., Rohde, E., & Gimona, M. (2020). Extracellular vesicles from human multipotent stromal cells protect against hearing loss after noise trauma in vivo. *Clinical and Translational Medicine*, 10, e262.
- Warnecke, A., Prenzler, N., Harre, J., Köhl, U., Gärtnertner, L., Lenarz, T., Laner-Plamberger, S., Wietzorrek, G., Staecker, H., Lassacher, T., Hollerweger, J., Gimona, M., & Rohde, E. (2021). First-in-human intracochlear application of human stromal cell-derived extracellular vesicles. *Journal of Extracellular Vesicles*, 10, e12094.
- Wiklander, O. P. B., Bostancioglu, R. B., Welsh, J. A., Zickler, A. M., Murke, F., Corso, G., Felldin, U., Hagey, D. W., Evertsson, B., Liang, X. M., Gustafsson, M. O., Mohammad, D. K., Wiek, C., Hanenberg, H., Bremer, M., Gupta, D., Björnstedt, M., Giebel, B., Nordin, J. Z., ... Görgens, A. (2018). Systematic methodological evaluation of a multiplex bead-based flow cytometry assay for detection of extracellular vesicle surface signatures. *Frontiers in Immunology*, 9, 1326.
- Wiklander, O. P. B., Brennan, M. Å., Lötvall, J., Breakefield, X. O., & El Andaloussi, S. (2019). Advances in therapeutic applications of extracellular vesicles. *Science Translational Medicine*, 11, eaav8521.
- Wu, Z., Zhang, S., Zhou, L., Cai, J., Tan, J., Gao, X., Zeng, Z., & Li, D. (2017). Thromboembolism induced by umbilical cord mesenchymal stem cell infusion: A report of two cases and literature review. *Transplantation Proceedings*, 49, 1656–1658.
- Yang, Z., Xie, J., Zhu, J., Kang, C., Chiang, C., Wang, X., Wang, X., Kuang, T., Chen, F., Chen, Z., Zhang, A., Yu, B., Lee, R. J., Teng, L., & Lee, L. J. (2016). Functional exosome-mimic for delivery of siRNA to cancer: In vitro and in vivo evaluation. *Journal of Controlled Release*, 243, 160–171.
- Yeo, R. W. Y., Lai, R. C., Zhang, B., Tan, S. S., Yin, Y., Teh, B. J., & Lim, S. K. (2013). Mesenchymal stem cell: An efficient mass producer of exosomes for drug delivery. *Advanced Drug Delivery Reviews*, 65, 336–341.
- Zhai, X., Chen, K., Yang, H., Li, B., Zhou, T., Wang, H., Zhou, H., Chen, S., Zhou, X., Wei, X., Bai, Y., & Li, M. (2021). Extracellular vesicles derived from CD73 modified human umbilical cord mesenchymal stem cells ameliorate inflammation after spinal cord injury. *Journal of Nanobiotechnology*, 19, 274.

- Zhang, C., Mok, J., Seong, Y., Lau, H. C., Kim, D., Yoon, J., Oh, S. W., Park, T. S., & Park, J. (2021). PROKR1 delivery by cell-derived vesicles restores the myogenic potential of Prokr1-deficient C2C12 myoblasts. *Nanomedicine*, 37, 102448.
- Zhang, S., Chuah, S. J., Lai, R. C., Hui, J. H. P., Lim, S. K., & Toh, W. S. (2018). MSC exosomes mediate cartilage repair by enhancing proliferation, attenuating apoptosis and modulating immune reactivity. *Biomaterials*, 156, 16–27.
- Zhao, Q., Hai, B., Kelly, J., Wu, S., & Liu, F. (2021). Extracellular vesicle mimics made from iPS cell-derived mesenchymal stem cells improve the treatment of metastatic prostate cancer. *Stem Cell Research & Therapy*, 12, 29.
- Zhu, L., Gangadaran, P., Kalimuthu, S., Oh, J. M., Baek, S. H., Jeong, S. Y., Lee, S. W., Lee, J., & Ahn, B. C. (2018). Novel alternatives to extracellular vesicle-based immunotherapy - exosome mimetics derived from natural killer cells. *Artificial Cells, Nanomedicine, and Biotechnology*, 46, S166–S179.

SUPPORTING INFORMATION

Additional supporting information can be found online in the Supporting Information section at the end of this article.

How to cite this article: Lau, H. C., Han, D. W., Park, J., Lehner, E., Kals, C., Arzt, C., Bayer, E., Auer, D., Schally, T., Grasmann, E., Fang, H., Lee, J. Y., Lee, H. S., Han, J., Gimona, M., Rohde, E., Bae, S., & Oh, S. W. (2022). GMP-compliant manufacturing of biologically active cell-derived vesicles produced by extrusion technology. *Journal of Extracellular Biology*, 1, e70. <https://doi.org/10.1002/jex2.70>